Impedance learning for human-guided robots in contact with unknown environments

Xueyan Xing, Etienne Burdet, Weiyong Si, Chenguang Yang, *IEEE Senior Member*, and Yanan Li, *IEEE Senior Member*

***Abstract*—Previous works have developed impedance control to increase safety and improve performance in contact tasks, where the robot is in physical interaction with either an environment or a human user. This paper investigates impedance learning for a robot guided by a human user while interacting with an unknown environment. We develop automatic adaptation of robot impedance parameters to reduce the effort required to guide the robot through the environment, while guaranteeing interaction stability. For non-repetitive tasks, this novel adaptive controller can attenuate disturbances by learning appropriate robot impedance. Implemented as an iterative learning controller, it can compensate for position dependent disturbances in repeated movements. Experiments demonstrate that the robot controller can, in both repetitive and non-repetitive tasks: i) identify and compensate for the interaction, ii) ensure both contact stability (with reduced tracking error) and maneuverability (with less driving effort of the human user) in contact with real environments, and iii) is superior to previous velocity-based impedance adaptation control methods.**

***Index Terms*—Human-robot-environment interaction control; learning control; impedance control.**

NOMENCLATURE

$\boldsymbol{d}$ Environmental disturbance.
$\boldsymbol{M}, \boldsymbol{B}, \boldsymbol{g}$ Inertia, Coriolis coefficient, and gravity of the robot.
$\boldsymbol{u}$ Robot control input.
$\boldsymbol{v}$ Velocity of the robot end-effector.
$\boldsymbol{x}$ Position of the robot end-effector.
$\boldsymbol{\xi}$ Integration variable of space (for stability analysis).
$\boldsymbol{f_h}$ Interaction force between the human and robot.
$\boldsymbol{x_e}$ Rest position of the environment.
$\boldsymbol{x_h}, \boldsymbol{x_r}$ Reference positions of the human and robot.
$\boldsymbol{e_h}, \boldsymbol{e}$ Tracking errors of the human and robot.
$\boldsymbol{K_h}, \boldsymbol{K_{hv}}$ Stiffness and viscosity matrices of the human arm.
$\boldsymbol{K_s}, \boldsymbol{K_{vs}}, \boldsymbol{k_{ps}}, \boldsymbol{x_{es}}$ Spatial form of $\boldsymbol{K}, \boldsymbol{K_v}, \boldsymbol{k_p}, \boldsymbol{x_e}$.
J Index of driving effort of the human user.
V Lyapunov function of the system (for stability analysis).
$\boldsymbol{K}, \boldsymbol{K_v}, \boldsymbol{K_e}$ Coefficients of the disturbance and control matrix.
$\hat{\boldsymbol{K}}, \hat{\boldsymbol{K}}_{\boldsymbol{v}}, \hat{\boldsymbol{k}}_{\boldsymbol{p}}$ Estimations of $\boldsymbol{K}, \boldsymbol{K_v}, \boldsymbol{k_p}$, where $\boldsymbol{k_p} = -\boldsymbol{K}\boldsymbol{x_e}$.
a_j, b_j, c_j Parameters of the velocity-based adaptation in eq. (24)
P_E Capability of the method in terms of contact stability.
T_i ith iteration period for repetitive tasks.
$\boldsymbol{A}, \boldsymbol{A_v}, \boldsymbol{A_p}, \boldsymbol{\Lambda}$ Parameters of the proposed iterative impedance learning method.
$\boldsymbol{A_f}, \boldsymbol{A_d}, \boldsymbol{A_c}$ Parameters of the proposed adaptive impedance learning method.
η, μ Parameters of the improved $\boldsymbol{\Lambda}$.
$\overline{T}$ Maximum iteration period for repetitive tasks.
σ Integration variable of time (for stability analysis).
E Total tracking error.
$\hat{\boldsymbol{K}}_{\boldsymbol{s}}, \hat{\boldsymbol{K}}_{\boldsymbol{vs}}, \hat{\boldsymbol{k}}_{\boldsymbol{ps}}$ Estimations of $\boldsymbol{K_s}, \boldsymbol{K_{vs}}, \boldsymbol{k_{ps}}$.
P_F Capability of the method in terms of maneuverability.

This work was supported in part by the U.K. EPSRC under Grant EP/T006951/1, in part by the (Chinese) State Key Laboratory of Robotics and Systems (HIT) under Grant SKLRS-2022-KF-16, and in part by the European Commission under Grant ICT-871803 CONBOTS. (Corresponding author: Yanan Li.)

This work involved human subjects or animals in its research. Approval of all ethical and experimental procedures and protocols was granted by (the Sciences and Technology Cross-Schools Research Ethics Committee of Sussex University and the UWE Faculty Research Ethics Committee) (IF PROVIDED under Application No. ER/YL557/1 and No. FET-2122-59, respectively).

Xueyan Xing and Yanan Li are with the Department of Engineering and Design, University of Sussex, BN1 9RH Brighton, U.K. (e-mail: xx92@sussex.ac.uk; yl557@sussex.ac.uk).

Etienne Burdet is with the Department of Bioengineering, Imperial College of Science, Technology and Medicine, SW7 2AZ London, U.K. (e-mail: eburdet@ic.ac.uk).

Weiyong Si and Chenguang Yang are with the Bristol Robotics Laboratory, University of the West of England, BS16 1QY Bristol, U.K. (e-mail: weiyong.si@uwe.ac.uk; cyang@ieee.org).

I. INTRODUCTION

Various robotic applications, such as (tele)operating a microrobot, demand a robot to be guided by a human while interacting with the environment. Most existing robotic interaction control schemes focus on achieving an effective interaction either with the human operator, or with an environment. However, during the execution of many human-robot interaction tasks, the robot may concurrently interact with an environment, for example during human-guided tooling. This interaction may destabilise the movement, affect task performance, and fatigue the human operator. Our vision to avoid these shortcomings is for a robot to understand the human intention, while learning to compensate for identified reproducible interaction dynamics during movement.

When a human user guides a robot to complete a tooling task such as cutting, polishing, or drilling, they need to exert a force on the robot to move it along the planned trajectory and achieve satisfying tooling performance. For instance, as a human user carries out a carving task, they need to apply a certain force to manipulate the blade along a desired trajectory. If the engraved plate is of hard texture, there will be a large resistive disturbance that will degrade the carving performance. If the human user wants to maintain the carving quality, more effort is needed to overcome the unknown

disturbance. In this case, a robot that complies with human movement while concurrently attenuating environmental disturbance is required.

To analyze the interaction of the human operator with the robot and its environment, we define ***maneuverability*** as the degree of difficulty to guide the robot for completing a task in the presence of environmental perturbations. The more easily the human operator can guide the robot, the higher the maneuverability. We also define ***contact stability*** as the capability for the robot to ensure good task performance despite environmental perturbations. The robot should both i) allow the human operator to easily move and flexibly operate the robot thus yielding high maneuverability, and ii) complete the task with a small error in the presence of perturbation from the environment, such as vibration due to a nonhomogeneous material and undesirable friction, i.e. the contact stability has to be guaranteed. Usually, the contact stability is guaranteed at the expense of the maneuverability, or vice versa. When the human user tries to improve their performance, i.e., to reduce the tracking error, they need more effort to compensate for the disturbance, which will result in decreasing maneuverability. Conversely, with less human control effort, the task performance will be deteriorated due to the negative effects of the disturbance. In other words, maneuverability and contact stability are hard to ensure concurrently. Our goal is to develop an interaction controller that makes robots able to interact with their environment, while offering both high maneuverability and contact stability to the human operator.

A. Previous works in human-robot interaction

How to design a robot controller for *intuitive and efficient human-robot interaction* is a prevalent research topic in the robotics field. Robots that interact with humans to perform their functions include rehabilitation robots, robotic exoskeletons, collaborative robots (cobots) for micro manipulation and industrial assembly, and semi-autonomous vehicles. Impedance control is often used on these contact robots to yield a compliant interaction of a robot with its human operator.

Facing uncertain human behaviors, a number of works estimate the human impedance or intention to dynamically adjust the robot's impedance parameters for efficient and stable interaction. For instance, it has been proposed to regulate the robot impedance using muscle activity measured with surface electromyography, although the underlying control is limited by the large signal variability and neural constraints [1], [2]. To address these limitations, several approaches used the force and position information of the human limb, which can be directly measured by sensors, to infer their impedance and adjust the robot's impedance correspondingly [3], [4]. Other works estimate intention or characteristics of the human partner, e.g. trajectory in [5] or human impedance in [6], [7] for adjustment of the robot's impedance. Alternatively, a velocity-related heuristic rule scheme has been considered in [4], [8] to adjust robot impedance, rather than relying on the human partner's behaviour. In addition, several works considered that human movements obey a certain probability distribution that can be identified to infer their intention [9]. Based on time-series data, the motion intention was estimated using the sparse Bayesian learning method in [10], and an adaptive impedance control algorithm was developed for effective human-robot collaboration. Instead of adjusting the robot's impedance, the robot's reference trajectory can be updated to achieve efficient human-robot interaction [11]. A review of human-robot interaction control can be found in [12]. However, previous works do not explicitly consider concurrent interactions between the robot, human operator, and environment.

B. Existing works on robot-environment interaction

Contact tooling tasks by definition involve *a desired interaction between the robot and the environment.* Control theory has been used to consider robot-environment interaction stability, and to develop impedance adaptation. In [13]–[15], the interaction force between the robot and the human was considered as an environmental force, where neural and iterative learning controls were used to mitigate its negative effect. Different from [13]–[15], the adaptive control strategy in [16] could generate the desired interaction force between robot and environment by adjusting the feedforward force, impedance, and trajectory of the robot. Reinforcement learning approaches have also been proposed to determine the optimal impedance parameters of the robot controller to achieve desired robot-environment interaction performance [17]–[20]. A reward function including contact information, e.g. the interaction force, was used to determine the optimal impedance parameters of the robot controller to achieve desired robot-environment interaction performance [21]. Fuzzy logic controllers have also been developed for impedance adaptation of the robot. Based on a fuzzy neural network learning algorithm, an adaptive controller was designed in [22] for adjusting the impedance parameters of the robot so as to produce smooth control even during transitions from free movement to contact. However, the controllers designed in [13]–[22] do not consider a human operator.

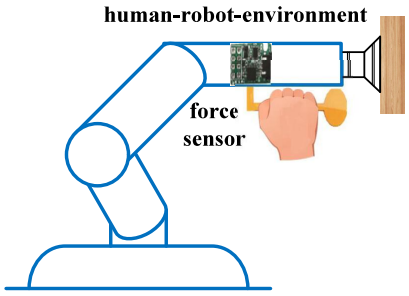

Fig. 1: Human-robot-environment interaction: A robot is guided by a human operator while in physical contact with an environment.

C. Contributions of this paper on human-robot-environment interaction

Different from the aforementioned works that considered either the interaction between robot and environment, or the

interaction between robot and human, we will consider here both the human operator and the environment. We will design a robot controller that automatically infers the intention of the human and adapts to an uncertain environment by learning the resulting impedance to improve the task performance. It is not a simple combination of two controllers for robot-environment interaction and human-robot interaction, as the two control objectives can be contradictory, leading to a conflicting trade-off between maneuverability and contact stability as discussed above. Our idea is to maintain the robot's maneuverability by inferring the human intent while only introducing additional impedance to deal with the environmental disturbance and thus ensure contact stability. As a result, both the maneuverability and the contact stability can be ensured during the human-robot-environment interaction, and the conflict between the human effort and the task performance is addressed.

The designed impedance learning strategy can be applied to both non-repetitive tasks, such as engraving or drawing, in the form of adaptive learning, and repetitive tasks, such as grinding or polishing, in the form of iterative learning. In the collaborative tasks considered in this paper, the robot is guided by the human user that assists them to complete a task in the presence of uncertain environmental disturbances. As illustrated by Fig. 1, the human user holds the robot and their interaction force can be measured by a force sensor. Simultaneously, the robot interacts with the environment for a certain tooling task. As the interaction force between the robot and the environment is typically subject to significant noise, it is not measured by a force sensor. Instead, due to repetitive interaction and periodicity of the environmental parameters, the disturbance from the environment can be learned by the robot.

The remaining of the paper is organized as follows: Section II formulates dynamics of and issues with the human-guided robot in contact with the environment. An adaptive variable impedance control is developed in Section III for non-repetitive tasks. Section IV presents an iterative control method with variable impedance learning for repetitive tasks considering position dependent disturbances. An experiment to test the algorithm's ability to identify a known virtual environment and yield stable interaction behavior is described in Section V. Section VI presents an experiment to test the effectiveness of the proposed impedance learning scheme in interaction with real environments. Section VII summarizes the contribution of this paper and analyzes the advantage of the proposed control method by comparing with the existing velocity-based adaptation method. The variables used in the paper are listed in Nomenclature.

II. Problem formulation

A. Dynamics of human-robot-environment interaction

We aim to design a controller for a human-guided robot that can stably interact with an environment. The dynamics of the n-degree of freedom (DoF) human-guided robot can be modelled as

$$\boldsymbol{M}\,\ddot{\boldsymbol{x}} + \boldsymbol{B}\,\dot{\boldsymbol{x}} + \boldsymbol{g} = \boldsymbol{f_h} + \boldsymbol{d} + \boldsymbol{u}, \tag{1}$$

where $\boldsymbol{x} = [x_1, \cdots, x_n]^{\mathrm{T}} \in \mathbb{R}^n$ is the position vector of the end-effector, $\boldsymbol{M} \in \mathbb{R}^{n\times n}$ the inertia matrix of the robot, $\boldsymbol{B} \in \mathbb{R}^{n\times n}$ the positive definite matrix related to the Coriolis force, $\boldsymbol{g} \in \mathbb{R}^n$ the gravity force on the robot, $\boldsymbol{f_h} \in \mathbb{R}^n$ the vector of the measured interaction force signals, $\boldsymbol{d} \in \mathbb{R}^n$ disturbance due to the interaction with an unknown environment, and $\boldsymbol{u} \in \mathbb{R}^n$ the robot command vector. In the model in eq. (1), parameters of the robot $\boldsymbol{M}, \boldsymbol{B}, \boldsymbol{g}$ are time-varying and state-related, but their arguments are omitted in this paper to facilitate the readability.

In this paper, the human force $\boldsymbol{f_h}$ is expected to be minimised, even with an environmental disturbance $\boldsymbol{d}$. While both $\boldsymbol{f_h}$ and $\boldsymbol{d}$ are external forces on the robot controller, $\boldsymbol{f_h}$ is considered 'desirable' as it indicates the human's planned trajectory and $\boldsymbol{d}$ is 'undesirable' as it may cause instability.

The interaction force can be modelled as [23]

$$\boldsymbol{f_h} = \boldsymbol{M}\,\ddot{\boldsymbol{x}}_{\boldsymbol{h}} + \boldsymbol{B}\,\dot{\boldsymbol{x}}_{\boldsymbol{h}} - \boldsymbol{K_h}\,\boldsymbol{e_h} - \boldsymbol{K_{hv}}\,\dot{\boldsymbol{e}}_{\boldsymbol{h}}, \boldsymbol{e_h} = \boldsymbol{x} - \boldsymbol{x_h}, \tag{2}$$

where $\boldsymbol{x_h} \in \mathbb{R}^n$ is the desired position vector of the human that is unknown to the robot, $\boldsymbol{K_h} \in \mathbb{R}^{n\times n}$ and $\boldsymbol{K_{hv}} \in \mathbb{R}^{n\times n}$ are stiffness and viscosity matrices of the human arm and $\boldsymbol{e_h} \in \mathbb{R}^n$ is the tracking error between $\boldsymbol{x_h}$ and $\boldsymbol{x}$. The first two terms of eq. (2) correspond to the feedforward force to compensate for the system dynamics and the last two terms to muscle viscoelasticity. Notice that eq. (2) is not used in the following robot controller design, but only for analysis purpose. If the robot is without disturbance and only with gravity compensation, i.e. $\boldsymbol{d} = \boldsymbol{0}$ and $\boldsymbol{u} = \boldsymbol{g}$, then combining eqs. (1,2) yields

$$\boldsymbol{M}\,\ddot{\boldsymbol{e}}_{\boldsymbol{h}} + (\boldsymbol{B} + \boldsymbol{K_{hv}})\dot{\boldsymbol{e}}_{\boldsymbol{h}} + \boldsymbol{K_h}\,\boldsymbol{e_h} = \boldsymbol{0}\,, \tag{3}$$

which shows that the robot can stably follow $\boldsymbol{x_h}$ corresponding to the human's motion intent and the instability in practice is largely caused by the environmental disturbance.

Since the human force can guide the robot to the desired position without disturbance and control, under such an ideal case, the robot passively follows the desired human trajectory as expected and $\boldsymbol{e_h} \approx \boldsymbol{0}$. Then using eq. (2), we have

$$\boldsymbol{M}\,\ddot{\boldsymbol{x}}_{\boldsymbol{h}} + \boldsymbol{B}\,\dot{\boldsymbol{x}}_{\boldsymbol{h}} = \boldsymbol{f_h}\,. \tag{4}$$

If we define the reference position vector of the robot as $\boldsymbol{x_r} \in \mathbb{R}^n$, replacing $\boldsymbol{x_h}$ in eq. (4) with $\boldsymbol{x_r}$ yields

$$\boldsymbol{M}\,\ddot{\boldsymbol{x}}_{\boldsymbol{r}} + \boldsymbol{B}\,\dot{\boldsymbol{x}}_{\boldsymbol{r}} = \boldsymbol{f_h}\,. \tag{5}$$

With eq. (5), the reference trajectory of the robot $\boldsymbol{x_r}$ is available for the impedance control designed in the following sections.

B. Stability analysis for human-robot-environment interaction

This section analyzes the system stability to develop an impedance learning controller for an ideal case with measurable disturbance. Let us consider a general visco-elastic model of the environment:

$$\boldsymbol{d} = \boldsymbol{K}(\boldsymbol{x} - \boldsymbol{x_e}) + \boldsymbol{K_v}\,\dot{\boldsymbol{x}}\,, \tag{6}$$

where $\boldsymbol{K} \in \mathbb{R}^{n\times n}$ and $\boldsymbol{K_v} \in \mathbb{R}^{n\times n}$ are the coefficients of the disturbance and $\boldsymbol{x_e} \in \mathbb{R}^n$ is the rest position of the environment.

When there is no external disturbance and the robotic control is designed only for gravity compensation, i.e. $\boldsymbol{u} = \boldsymbol{g}$ and $\boldsymbol{d} = \boldsymbol{0}$, according to eq. (1)

$$\boldsymbol{M}\,\ddot{\boldsymbol{x}} + \boldsymbol{B}\,\dot{\boldsymbol{x}} = \boldsymbol{f_h} \tag{7}$$

in which $\boldsymbol{f_h}$ is driving the robot toward $\boldsymbol{x_h}$ as shown in eq. (4) and the interaction system is stable if eq. (7) holds.

If only the gravity compensation is considered in the robotic controller, considering the system in eq. (1) with $\boldsymbol{u} = \boldsymbol{g}$ and the disturbance $\boldsymbol{d}$ in eq. (6), the model of the human-guided robot can be rewritten as

$$\boldsymbol{M}\,\ddot{\boldsymbol{x}} + \bar{\boldsymbol{B}}\,\dot{\boldsymbol{x}} + \bar{\boldsymbol{C}}\,\boldsymbol{x} + \bar{\boldsymbol{a}} = \boldsymbol{f_h}\,, \tag{8}$$

where

$$\bar{\boldsymbol{B}} = \boldsymbol{B} - \boldsymbol{K_v}\,, \quad \bar{\boldsymbol{C}} = -\boldsymbol{K}\,, \quad \bar{\boldsymbol{a}} = \boldsymbol{K}\,\boldsymbol{x_e}. \tag{9}$$

It is clear that when the disturbance is resistive to the robot movement, i.e. the matrices $\boldsymbol{K}$ and $\boldsymbol{K_v}$ are positive definite, the human-guided robot in eq. (8) could become unstable in the presence of large disturbances because of the undesired terms $\bar{\boldsymbol{B}}$, $\bar{\boldsymbol{C}}\,\boldsymbol{x}$ and $\bar{\boldsymbol{a}}$ in eq. (9), such that more human effort is needed for a stable contact. Therefore, to achieve a stable contact with the environment while maintaining the robot's maneuverability, a robotic controller is required to attenuate the effect of the disturbance.

According to the model in eq. (1), if the environmental disturbance d is measurable, a robot controller with gravity compensation can be designed as

$$\boldsymbol{u} = -\boldsymbol{d} + \boldsymbol{g} \tag{10}$$

such that eq. (7) holds even with the disturbance. This would enable the human to use little effort to ensure the contact stability and guide the robot. In practical operation, the environmental disturbance is hard to be accurately estimated. In the next two sections, an impedance controller is designed based on the human-guided robot model in eq. (1), which does not require knowledge of $\boldsymbol{d}$ and $\boldsymbol{x_h}$ to guarantee the contact stability and the robot maneuverability.

III. Impedance control design for non-repetitive tasks

For the non-repetitive task considered in this section, the coefficients $\boldsymbol{K}$ and $\boldsymbol{K_v}$ of the disturbance in eq. (6) and the rest position of the environment $\boldsymbol{x_e}$ are constant. Then an adaptive impedance control is designed as

$$\boldsymbol{u} = -\hat{\boldsymbol{K}}\,\boldsymbol{x} - \hat{\boldsymbol{K}}_{\boldsymbol{v}}\,\dot{\boldsymbol{x}} - \hat{\boldsymbol{k}}_{\boldsymbol{p}} - \boldsymbol{K_e}\dot{\boldsymbol{e}} + \boldsymbol{g} \tag{11}$$

with impedance learning laws

$$\dot{\hat{\boldsymbol{K}}} = \dot{\boldsymbol{e}}\,\boldsymbol{x}^{\mathrm{T}}\boldsymbol{A_f}\,, \quad \dot{\hat{\boldsymbol{K}}}_{\boldsymbol{v}} = \dot{\boldsymbol{e}}\,\dot{\boldsymbol{x}}^{\mathrm{T}}\boldsymbol{A_d}\,, \quad \dot{\hat{\boldsymbol{k}}}_{\boldsymbol{p}} = \boldsymbol{A_c}\,\dot{\boldsymbol{e}}, \tag{12}$$

where $\boldsymbol{e} \in \mathbb{R}^n$ is the tracking error of the robot

$$\boldsymbol{e} = \boldsymbol{x} - \boldsymbol{x_r}\,, \tag{13}$$

and $\boldsymbol{A_f}$, $\boldsymbol{A_d}$, $\boldsymbol{A_c}, \boldsymbol{K_e} \in \mathbb{R}^{n\times n}$ are positive definite diagonal matrices.

Eq. (12) can be used to compute $\hat{\boldsymbol{K}}$, $\hat{\boldsymbol{K}}_{\boldsymbol{v}}$, and $\hat{\boldsymbol{k}}_{\boldsymbol{p}}$ for the control of eq. (11). For example, $\hat{\boldsymbol{K}}$ can be computed from $\hat{\boldsymbol{K}}\,(t+\Delta t) = \dot{\boldsymbol{e}}\boldsymbol{x}^{\mathrm{T}}\boldsymbol{A_f}\Delta t + \hat{\boldsymbol{K}}\,(t)$ using Euler integration with a predefined initial value $\hat{\boldsymbol{K}}\,(0)$, where Δt denotes the sampling time. In eq. (12), we know that $\hat{\boldsymbol{K}}$, $\hat{\boldsymbol{K}}_{\boldsymbol{v}}$, and $\hat{\boldsymbol{k}}_{\boldsymbol{p}}$ update depending on the variation speed of the tracking error $\dot{\boldsymbol{e}}$, and the position $\boldsymbol{x}$ and velocity $\dot{\boldsymbol{x}}$ of the system. Since the disturbance $\boldsymbol{d}$ in eq. (6) can be rewritten as $\boldsymbol{d} = \boldsymbol{K}\boldsymbol{x} - \boldsymbol{K}\boldsymbol{x_e} + \boldsymbol{K_v}\,\dot{\boldsymbol{x}}$, it is related to the position $\boldsymbol{x}$, the velocity $\dot{\boldsymbol{x}}$ of the system, as well as the rest position of the environment $\boldsymbol{x_e}$. As a result, the controller will update its three parameters according to the current tracking performance, which is indicated by $\dot{\boldsymbol{e}}$, and the current degree of disturbance, which is indicated by $\boldsymbol{x}$ and $\dot{\boldsymbol{x}}$. Besides, according to the backward difference method, $\dot{\boldsymbol{x}}_{\boldsymbol{r}}$ can be represented as $\dot{\boldsymbol{x}}_{\boldsymbol{r}} = \frac{\boldsymbol{x_r}(t)-\boldsymbol{x_r}(t-\Delta t)}{\Delta t}$, where Δt is the sampling time and thus $\ddot{\boldsymbol{x}}_{\boldsymbol{r}} = \frac{\boldsymbol{x_r}(t)-2\boldsymbol{x_r}(t-\Delta t)+\boldsymbol{x_r}(t-2\Delta t)}{(\Delta t)^2}$ according to [24]. By substituting the expressions of $\dot{\boldsymbol{x}}_{\boldsymbol{r}}$ and $\ddot{\boldsymbol{x}}_{\boldsymbol{r}}$ into eq. (5), the reference trajectory of the robot $\boldsymbol{x_r}\,(t)$ used in eq. (13) can be updated using $\boldsymbol{x_r}\,(t) = \left[(\Delta t)^2\boldsymbol{f_h} - \boldsymbol{M}\boldsymbol{x_r}\,(t-2\Delta t) + (\boldsymbol{B}\Delta t + 2\boldsymbol{M})\,\boldsymbol{x_r}\,(t-\Delta t)\right] \times (\boldsymbol{M}+\boldsymbol{B}\Delta t)^{-1}$.

Substituting eq. (11) into eq. (1) yields

$$\boldsymbol{M}\,\ddot{\boldsymbol{x}} + (\boldsymbol{B} + \hat{\boldsymbol{K}}_{\boldsymbol{v}})\dot{\boldsymbol{x}} + \hat{\boldsymbol{K}}\,\boldsymbol{x} + \boldsymbol{K_e}\dot{\boldsymbol{e}} + \hat{\boldsymbol{k}}_{\boldsymbol{p}} = \boldsymbol{f_h} + \boldsymbol{d} \tag{14}$$

which can be rewritten as

$$\boldsymbol{M}\,\ddot{\boldsymbol{x}} + \check{\boldsymbol{B}}\,\dot{\boldsymbol{x}} + \check{\boldsymbol{C}}\,\boldsymbol{x} + \boldsymbol{K_e}\dot{\boldsymbol{e}} + \check{\boldsymbol{a}} = \boldsymbol{f_h} + \boldsymbol{d}\,, \tag{15}$$

where

$$\check{\boldsymbol{B}} \equiv \boldsymbol{B} + \hat{\boldsymbol{K}}_{\boldsymbol{v}}\,, \quad \check{\boldsymbol{C}} \equiv \hat{\boldsymbol{K}}\,, \quad \check{\boldsymbol{a}} \equiv \hat{\boldsymbol{k}}_{\boldsymbol{p}}\,. \tag{16}$$

From eq. (16), it is clear that the impedance matrices $\check{\boldsymbol{B}}$, $\check{\boldsymbol{C}}$, $\check{\boldsymbol{a}}$ are regulated according to the variation of the disturbance $\boldsymbol{d}$ with learning laws in eq. (12). When $\hat{\boldsymbol{K}}\boldsymbol{x} + \hat{\boldsymbol{K}}_{\boldsymbol{v}}\dot{\boldsymbol{x}} + \hat{\boldsymbol{k}}_{\boldsymbol{p}} \simeq \boldsymbol{K}\boldsymbol{x} + \boldsymbol{K_v}\dot{\boldsymbol{x}} - \boldsymbol{K}\,\boldsymbol{x_e}$, eq. (7) holds with an additional assistive force $\boldsymbol{K_e}\dot{\boldsymbol{e}}$ provided by the robot such that the human can guide the robot with $\boldsymbol{f_h}$ free from the disturbance.

Using eqs. (5,6,11), eq. (1) can be rewritten as

$$\boldsymbol{M}\,\ddot{\boldsymbol{e}} + (\boldsymbol{B} + \boldsymbol{K_e})\,\dot{\boldsymbol{e}} = \tilde{\boldsymbol{K}}\,\boldsymbol{x} + \tilde{\boldsymbol{K}}_{\boldsymbol{v}}\,\dot{\boldsymbol{x}} + \tilde{\boldsymbol{k}}_{\boldsymbol{p}}\,, \tag{17}$$

where $\tilde{\boldsymbol{K}}$, $\tilde{\boldsymbol{K}}_{\boldsymbol{v}} \in \mathbb{R}^{n\times n}$ and $\tilde{\boldsymbol{k}}_{\boldsymbol{p}} \in \mathbb{R}^n$ are defined as

$$\tilde{\boldsymbol{K}} = \boldsymbol{K} - \hat{\boldsymbol{K}},\ \tilde{\boldsymbol{K}}_{\boldsymbol{v}} = \boldsymbol{K_v} - \hat{\boldsymbol{K}}_{\boldsymbol{v}},\ \tilde{\boldsymbol{k}}_{\boldsymbol{p}} = \boldsymbol{k_p} - \hat{\boldsymbol{k}}_{\boldsymbol{p}}, \tag{18}$$

while $\boldsymbol{k_p} = -\boldsymbol{K}\,\boldsymbol{x_e}$.

Using these notations, we can formulate ***Theorem 1***: For an n-DoF human-guided robot used in a non-repetitive task, the adaptive impedance control strategy in eqs. (11,12) can eliminate the adverse effect of the disturbance $\boldsymbol{d}$ and regulate the robot behavior so that the stability of the closed-loop system in eqs. (17,18) is guaranteed in the presence of $\boldsymbol{d}$. The proof of Theorem 1 is provided in Appendix 1.

Theorem 1 indicates that the disturbance can be learned using our adaptive impedance control scheme, thus the controller in eq. (11) enables eq. (7) to hold for the closed-loop interaction system. As impedance learning in eq. (12)

regulates the robot impedance to compensate for the effect of the disturbance during the interaction, the human user does not need to overcome the contact instability caused by the disturbance, and the effort to steer the robot is reduced. The above control process can be found in Fig. 2.

In eq. (11), $\boldsymbol{u}$ is derived by analyzing the stability of the disturbed human-robot-environment interaction system based on Lyapunov's stability theory [25]. We first need to select a Lyapunov function of the system (V in eq. (32) in Appendix 1) that includes the tracking error and the estimation error of the disturbance parameters that we want to minimize, then $\boldsymbol{u}$ is designed to make the controlled system stable through $\dot{V} \leq 0$.

For the designed control $\boldsymbol{u}$, the initial values of the estimated control parameters in eq. (11), $\hat{\boldsymbol{K}}(0)$, $\hat{\boldsymbol{K}}_{\boldsymbol{v}}(0)$, $\hat{\boldsymbol{k}}_{\boldsymbol{p}}(0)$, affect the transient performance but not the steady-state performance, and they are typically initialized as zero. However, the learning parameters $\boldsymbol{A_f}$, $\boldsymbol{A_d}$, $\boldsymbol{A_c}$ in eq. (12) should be manually tuned to be large enough to provide adequate convergence speed of the controlled system.

IV. Iterative impedance control for human-guided robot in repetitive tasks

When the robot performs a repetitive task, the environment has spatial periodicity, thus the disturbance can be considered as a function of the position as discussed in [26]. To further elaborate, instead of constant matrices, coefficients of the disturbance are spatially periodic, i.e. their values are the same for the same position in different iterations. We modify here the adaptive impedance control proposed in Section III for repetitive tasks, making it suitable for space-related disturbances with varying coefficients. The subscript $\boldsymbol{s}$ is used for space-related variables and time-related variables are without $\boldsymbol{s}$. The subscript i of a variable denotes its iteration number.

In the ith iteration, the spacial form of the environmental disturbance $\boldsymbol{d}_i$ in eq. (6) is written as

$$\boldsymbol{d}_i = \boldsymbol{K_s}(\boldsymbol{x}_i - \boldsymbol{x_{es}}) + \boldsymbol{K_{vs}}\,\dot{\boldsymbol{x}}_i, \tag{19}$$

where $\boldsymbol{K_s}$, $\boldsymbol{K_{vs}} \in \mathbb{R}^{n\times n}$ and $\boldsymbol{x_{es}} \in \mathbb{R}^n$ are the spatial form of $\boldsymbol{K}$, $\boldsymbol{K_v}$ and $\boldsymbol{x_e}$, respectively, which satisfy $\boldsymbol{K_{s},_i} = \boldsymbol{K_{s},_{i-1}}$, $\boldsymbol{K_{vs},_i} = \boldsymbol{K_{vs},_{i-1}}$, $\boldsymbol{x_{es},_i} = \boldsymbol{x_{es},_{i-1}}$.

Based on the disturbance in eq. (19), the robot control $\boldsymbol{u}$ is redesigned as

$$\boldsymbol{u}_i = -\hat{\boldsymbol{K}}_i\,\boldsymbol{x}_i - \hat{\boldsymbol{K}}_{\boldsymbol{v},i}\,\dot{\boldsymbol{x}}_i - \hat{\boldsymbol{k}}_{\boldsymbol{p},i} - \boldsymbol{K_e}\dot{\boldsymbol{e}}_i + \boldsymbol{g}, \tag{20}$$

where the control parameter matrix $\boldsymbol{K_e} \in \mathbb{R}^{n\times n}$ keeps the same for each iteration, and impedance parameter matrices $\hat{\boldsymbol{K}}_i \in \mathbb{R}^{n\times n}$, $\hat{\boldsymbol{K}}_{\boldsymbol{v},i} \in \mathbb{R}^{n\times n}$, and $\hat{\boldsymbol{k}}_{\boldsymbol{p},i} \in \mathbb{R}^n$ are updated in time as

$$\hat{\boldsymbol{K}}_i = \begin{cases} \hat{\boldsymbol{K}}_{i-1} + \dot{\boldsymbol{e}}_i\,\boldsymbol{x}_i^{\mathrm{T}}\boldsymbol{A}\boldsymbol{\Lambda} & \text{for } t \in [0, T_i] \\ \hat{\boldsymbol{K}}_{i-1} & \text{for } t \in (T_i\,, \overline{T}\,], \end{cases}$$

$$\hat{\boldsymbol{K}}_{\boldsymbol{v},i} = \begin{cases} \hat{\boldsymbol{K}}_{\boldsymbol{v},i-1} + \dot{\boldsymbol{e}}_i\,\dot{\boldsymbol{x}}_i^{\mathrm{T}}\boldsymbol{A_v}\,\boldsymbol{\Lambda} & \text{for } t \in [0, T_i] \\ \hat{\boldsymbol{K}}_{\boldsymbol{v},i-1} & \text{for } t \in (T_i\,, \overline{T}\,], \end{cases}$$

$$\hat{\boldsymbol{k}}_{\boldsymbol{p},i} = \begin{cases} \hat{\boldsymbol{k}}_{\boldsymbol{p},i-1} + \boldsymbol{A_p}\,\boldsymbol{\Lambda}\,\dot{\boldsymbol{e}}_i & \text{for } t \in [0, T_i] \\ \hat{\boldsymbol{k}}_{\boldsymbol{p},i-1} & \text{for } t \in (T_i\,, \overline{T}\,], \end{cases} \tag{21}$$

where $\boldsymbol{A}$, $\boldsymbol{A_v}$ and $\boldsymbol{A_p}$ are $\mathbb{R}^{n\times n}$ diagonal matrices with positive constant elements, $T_i \in [0, \overline{T}\,]$ is the actual learning time of the ith iteration, $\overline{T}$ is the maximum iteration period, $\boldsymbol{\Lambda} = \mathrm{diag}\{\lambda^1 \cdots \lambda^n\} \in \mathbb{R}^{n\times n}$ in which $\lambda^j = \left|v^j\right|^{-1}$ and $v^j \in \mathbb{R}$ is the current robot velocity along the jth dimension, $j = 1, \cdots, n$.

In traditional iterative learning control, a fixed iteration period is needed to ensure system stability. However, humans never repeat a movement with exactly the same time duration [27]. In our proposed method, the learning laws in eq. (21) are designed as piecewise functions. Based on this, we use the method in [15] and introduce $\boldsymbol{\Lambda}$ to deal with the varying iteration period. When the current velocity increases, the learning speed will correspondingly decrease due to the decrease of $\boldsymbol{\Lambda}$, so that the possible spatial inconsistency caused by the varying velocity can be corrected with our proposed update laws, and the stability of the human-robot-environment interaction system can be guaranteed. With the maximum iteration period $\overline{T}$, the controller updates its coefficients for $t \in [0, T_i]$ and stops updating for the rest of the duration since there is no valuable information to be learned. $\overline{T}$ could be theoretically set to be large enough to cover all possibilities so that the actual learning time T_i can eventually achieve it in the sense of $\lim_{i\to\infty} T_i = \overline{T}$ [15], [28]. However, if $\overline{T}$ is too large, the control period will be correspondingly extended, which will reduce the control efficiency. Therefore, $\overline{T}$ should be determined according to the task execution time. In practice, $\overline{T}$ can be set slightly larger than the prescribed movement time (e.g. as 4'30" for a 4' planned duration) to guarantee that the task can be completed.

Substituting eqs. (5,6,20) into eq. (1) yields

$$\boldsymbol{M}\,\ddot{\boldsymbol{e}}_i + (\boldsymbol{B} + \boldsymbol{K_e})\,\dot{\boldsymbol{e}}_i = \tilde{\boldsymbol{K}}_i\,\boldsymbol{x}_i + \tilde{\boldsymbol{K}}_{\boldsymbol{v},i}\,\dot{\boldsymbol{x}}_i + \tilde{\boldsymbol{k}}_{\boldsymbol{p},i}, \tag{22}$$

where $\tilde{\boldsymbol{K}}_i$, $\tilde{\boldsymbol{K}}_{\boldsymbol{v},i} \in \mathbb{R}^{n\times n}$ and $\tilde{\boldsymbol{k}}_{\boldsymbol{p},i} \in \mathbb{R}^n$ are defined as

$$\tilde{\boldsymbol{K}}_i = \boldsymbol{K}_i - \hat{\boldsymbol{K}}_i,\ \tilde{\boldsymbol{K}}_{\boldsymbol{v},i} = \boldsymbol{K}_{\boldsymbol{v},i} - \hat{\boldsymbol{K}}_{\boldsymbol{v},i},\ \tilde{\boldsymbol{k}}_{\boldsymbol{p},i} = \boldsymbol{k}_{\boldsymbol{p},i} - \hat{\boldsymbol{k}}_{\boldsymbol{p},i}, \tag{23}$$

where $\boldsymbol{k}_{\boldsymbol{p},i} = -\boldsymbol{K}_i\,\boldsymbol{x}_{\boldsymbol{e},i}$.

With above-mentioned equations, we can formulate ***Theorem 2***: For the n-DoF human-guided robot described by eq. (1) in repetitive tasks, the iterative impedance control strategy in eq. (20) with impedance learning laws in eq. (21) can guarantee the stability of the closed-loop system in eqs. (22, 23) in the presence of environmental disturbance, i.e. eq. (7) is satisfied with the proposed control. The proof of this

theorem is presented in Appendix 2, where the robot control is first designed to be space-related to conform with eq. (19) and then transformed to time domain for implementation.

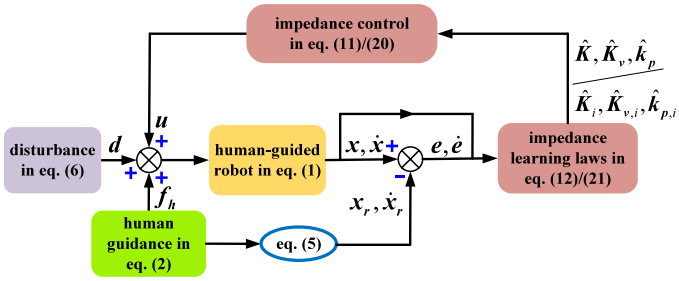

Fig. 2: Control block diagram of the human-guided robot for non-repetitive and repetitive tasks.

The block diagram of the resulting human-guided robot control for repetitive tasks is shown in Fig. 2. In order to avoid $\hat{\boldsymbol{K}}$, $\hat{\boldsymbol{K}}_{\boldsymbol{v}}$, and $\hat{\boldsymbol{k}}_{\boldsymbol{p}}$ becoming too large when the robot velocity is close to zero, λ^j defined in eq. (21) can be revised with $\lambda^j = \begin{cases} |v^j|^{-1}, & \text{if } |v^j| \geq \mu \\ (|v^j| + \eta)^{-1}, & \text{if } |v^j| < \mu \end{cases}$, where a constant η is added to λ^j when $|v^j|$ is less than a positive constant μ.

V. Control Validation with H-MAN Robot

To test the ability of the proposed impedance controller to identify the environmental disturbances and stably compensate for it, an experiment was implemented on a planar H-MAN robot with a virtual, software designed disturbance. The experiment was approved by the Sciences and Technology Cross-Schools Research Ethics Committee of Sussex University, UK (reference number ER/YL557/1). Six human subjects without known sensorimotor impairment were recruited, who all gave their informed consent prior to participating. International units are used in the following, unless specified.

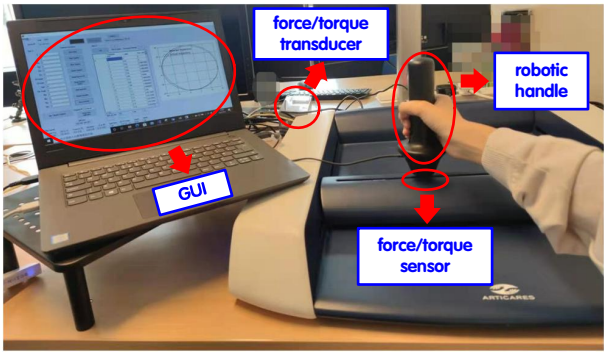

Fig. 3: Experimental setup with H-MAN robot to test the algorithm on a virtual environment interaction.

The experimental setup with the planar H-MAN robot is shown in Fig. 3. A graphical user interface (GUI) is designed to display the target trajectory and the cursor indicating the handle's position. In the experiment, the human operator holds the handle and guides the robot to track the target trajectory with the cursor on the GUI. The H-MAN robot is equipped with an ATI Mini 40 force/torque sensor at the handle. Since the virtual disturbance is introduced in software as a part of the control input of the robot (instead of stemming from interaction with a physical environment), the force measured by the load cell is only from the human.

To evaluate our proposed adaptive impedance control, the following three control conditions were compared:

- *Control off*: The robot control is 0;
- *Velocity-based:* The velocity-based impedance adaptation proposed in [4]:

$$u_j = -\min\left\{a_j\, e^{-b_j|\dot{x}_j|}, c_j\right\}\dot{x}_j\,,\ \ a_j, b_j, c_j > 0 \quad (24)$$

  where $j = 1, 2$ stands for x or y axis;
- *Impedance learning:* The proposed control method with impedance learning was used.

Each subject was instructed on how to use the H-MAN robot, and then practiced the task. Recording began when the subject felt confident in performing the task. Each subject carried out five trials in each of the three control conditions, whose order is unknown to them.

Sections V.A-C present the results of a representative subject, and the overall performance of the six subjects is described in Section V-D.

A. Non-repetitive task

In the non-repetitive task, the target displayed on the GUI moved in a circular trajectory $\left[10\cos(\frac{\pi}{4.5}t) \quad 10\sin(\frac{\pi}{4.5}t)\right]^{\mathrm{T}}$ cm. One trial consisted of tracking this trajectory once. The disturbance was set as $\boldsymbol{d} = \left[d_x \quad d_y\right]^{\mathrm{T}} = \left[20\,x_1 + 4\,\dot{x}_1 \quad 20\,x_2 + 4\,\dot{x}_2\right]^{\mathrm{T}}$ N.

The velocity-based control in eq. (24) was implemented with $a_1 = a_2 = 500$, $b_1 = b_2 = 3$ and $c_1 = c_2 = 50$. Impedance learning was implemented using the controller in eqs. (11,12) with parameters $\boldsymbol{K_e} = 0.1\,\boldsymbol{I}_2$, $\boldsymbol{A_f} = 0.5\,\boldsymbol{I}_2$, $\boldsymbol{A_d} = \boldsymbol{I}_2$, $\boldsymbol{A_c} = 0.05\,\boldsymbol{I}_2$, where $\boldsymbol{I}_2 = \begin{bmatrix}1 & 0\\ 0 & 1\end{bmatrix}$.

The maneuverability defined in this paper was evaluated using the l_2-norm of the instantaneous tracking error $\|\boldsymbol{e}\|$, while the contact stability was measured using the human effort, J, to drive the robot

$$J = \int_0^{T_0} |\boldsymbol{f}_{\boldsymbol{h}}^{\mathrm{T}}(t)\boldsymbol{v}(t)|\,\mathrm{d}t, \quad (25)$$

where T_0 is the task duration and $\boldsymbol{v}$ is the velocity of the interaction system. To evaluate the disturbance identification, the learned two-dimension disturbance $\hat{\boldsymbol{d}}$ for non-repetitive tasks

$$\hat{\boldsymbol{d}} = \left[\hat{d}_x \quad \hat{d}_y\right]^{\mathrm{T}} = \hat{\boldsymbol{K}}\,\boldsymbol{x} + \hat{\boldsymbol{K}}_{\boldsymbol{v}}\,\dot{\boldsymbol{x}} + \hat{\boldsymbol{k}}_{\boldsymbol{p}} \quad (26)$$

can be analyzed, where $\hat{\boldsymbol{K}}$, $\hat{\boldsymbol{K}}_{\boldsymbol{v}}$, $\hat{\boldsymbol{k}}_{\boldsymbol{p}}$ are coefficients of the disturbance learned according to eq. (12).

Fig. 4a shows the trajectories of a representative subject in one trial. In Fig. 4a, the dashed black line, corresponding to the subject guiding the robot without control and without disturbance, serves as a reference for best possible guidance.

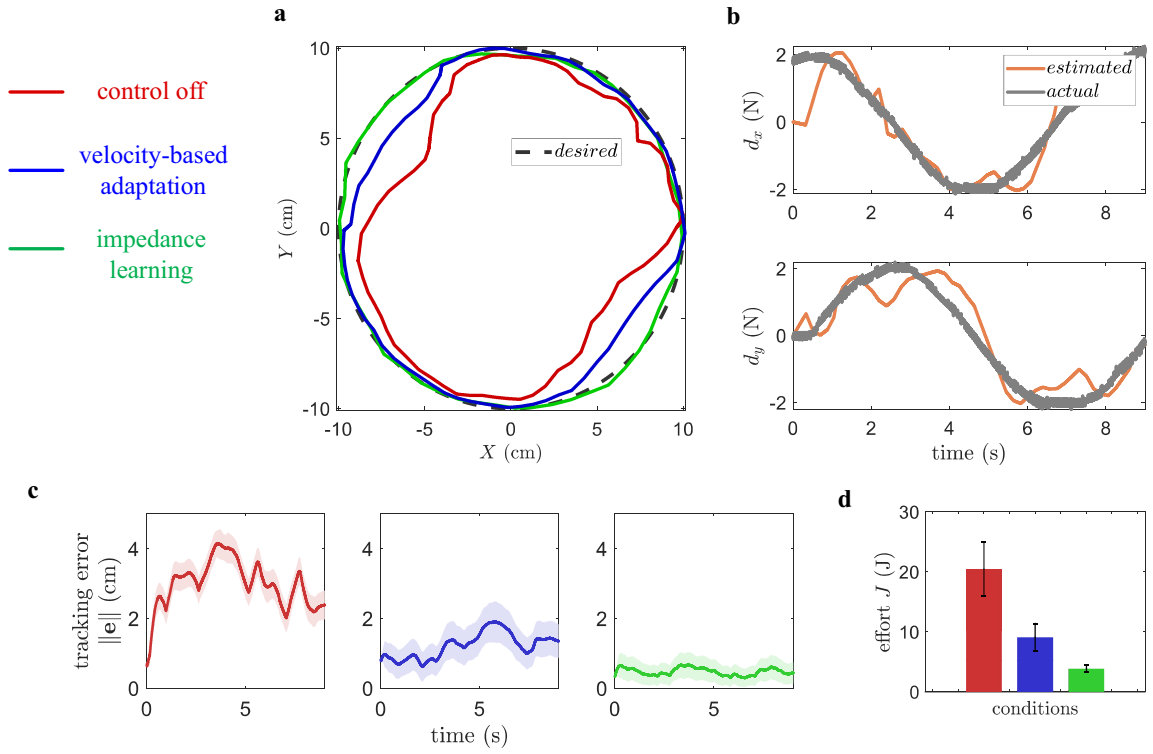

Fig. 4: Results of a representative subject for the non-repetitive task with the H-MAN robot, in the conditions of control off (in red), velocity-based adaptation (blue) and with the proposed adaptive impedance learning method (green). a: Actual trajectories over one trial in each condition. b: Average learned and actual disturbance. c: Average tracking error magnitude with ± standard deviation (std) error bars. d: Average effort of the user with ± std error bars.

This reference trajectory slightly deviates from the 10 cm radius circle, due to the H-MAN sensing error from cable deformation and to the variability of exerted force. We see in Fig. 4a that in the control off condition the disturbance largely affects the tracking error performance so that an effective control strategy is necessary to mitigate this negative effect. Although the velocity-based impedance adaptation improves the tracking performance, there is still tracking error with this method which does not model the environment interaction. Figs. 4c,d suggest that the proposed impedance learning controller yields better tracking performance while decreasing the effort to drive the robot for tracking the moving target. This arises as this controller accurately identifies the virtual environment. Fig. 4b indeed shows that the disturbance $\boldsymbol{d}$ is well identified.

B. Repetitive task

In the repetitive task, one trial consists of guiding the robot during four iterations to track a target moving on a smaller circle. The target trajectory is defined as $\begin{bmatrix}5\cos(0.25\pi\, t) & 5\sin(0.25\pi\, t)\end{bmatrix}^{\mathrm{T}}$ cm in the presence of disturbance $\boldsymbol{d} = \begin{bmatrix}d_x & d_y\end{bmatrix}^{\mathrm{T}}$ N where $d_x = 28(\sin 160x)^2 x + 4(\sin 80x)^2 \dot{x}$ and $d_y = 28(\cos 240y)^2 y + 4(\cos 40y)^2 \dot{y}$.

In our experiment, when the human subject stopped at a position for the prescribed time, we consider that the human completed the task. Since T_i in our proposed method in eq. (21) is the time required by the human movement in the ith iteration to complete the movement, it is computed as the time recorded by the timer of the robot achieving speed below the specified threshold minus this prescribed time. The above-mentioned method of obtaining T_i is also adaptable for the experiment with Panda robot in Section VI-B.

The iterative impedance learning in eqs. (20,21) was implemented with the parameters $\boldsymbol{K_e} = 0.1\,\boldsymbol{I}_2$, $\boldsymbol{A} = \boldsymbol{I}_2$, $\boldsymbol{A_v} = \boldsymbol{A_p} = 0.05\,\boldsymbol{I}_2$, $\eta = 1$, $\mu = 0.01$, $\overline{T} = 24$ s. The iterative learning scheme was compared with the conditions of control off and velocity-based impedance adaptation in eq. (24) with parameters $a_1 = a_2 = 500$, $b_1 = b_2 = 2$, $c_1 = c_2 = 100$. The maneuverability and the contact stability were evaluated from the last iteration of the five trials, where the effort metric J in eq. (25) is restricted to the last iteration's period

$$J = \int_0^{T_m} |\boldsymbol{f}_{\boldsymbol{h},m}^{\mathrm{T}}(t)\, \boldsymbol{v}(t)|\, \mathrm{d}t, \tag{27}$$

where T_m is the last iteration's duration and m equals 4 for this experiment. Similarly, the learned disturbance in eq. (26) is redefined as

$$\hat{\boldsymbol{d}} = \begin{bmatrix}\hat{d}_x & \hat{d}_y\end{bmatrix}^{\mathrm{T}} = \hat{\boldsymbol{K}}_m\, \boldsymbol{x}_m + \hat{\boldsymbol{K}}_{\boldsymbol{v},m}\, \dot{\boldsymbol{x}}_m + \hat{\boldsymbol{k}}_{\boldsymbol{p},m}\,, \tag{28}$$

where $\hat{\boldsymbol{K}}_m$, $\hat{\boldsymbol{K}}_{\boldsymbol{v},m}$, $\hat{\boldsymbol{k}}_{\boldsymbol{p},m}$ are computed from eq. (21).

Fig. 5a shows the trajectory in the three control conditions over one trial of each subject. Here also the disturbance has a significant effect on tracking performance relative to the reference trajectory (without disturbance and without control) which is partly addressed by the velocity-based adaptation. In comparison, the proposed impedance learning method reduces the tracking error (Fig. 5c) to a minimum, and also

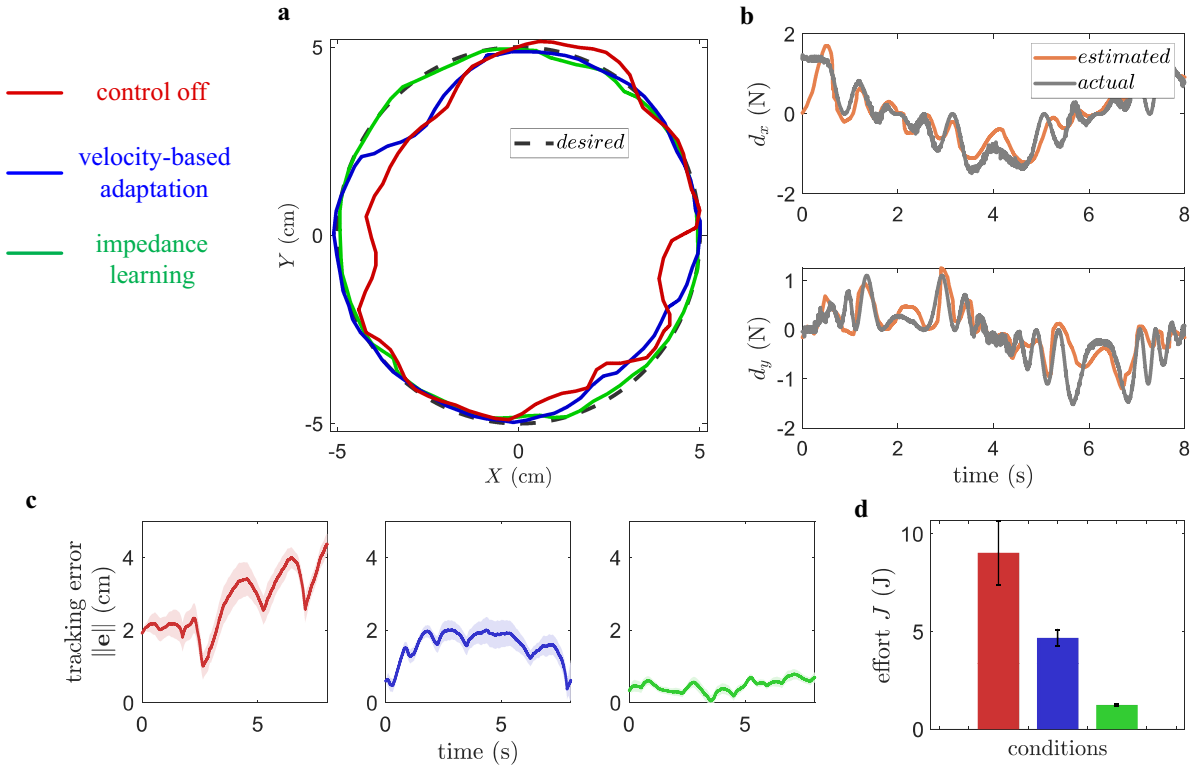

Fig. 5: Results for a repetitive task carried out by a representative subject (same subject as Fig. 4) with the H-MAN robot, in the three conditions of control off (red), with the velocity-based adaptation (blue) and with the proposed iterative impedance learning method in the last (4th) iteration (green). a: Actual trajectories over one trial. b: Average learned and actual disturbances. c: Average tracking error magnitude with ± std error bars. d: Average effort of the user with ± error std bars.

minimizes the effort to drive the robot (Fig. 5d). The average learned and the actual disturbance of four iterations are illustrated in Fig. 5b. We see that the disturbance learned by iterative impedance learning laws in eq. (21) converges to the actual values. In comparison with the non-repetitive tracking task above, the controller can now identify a more complex disturbance which contributes to the good performance of our proposed method.

C. Performance with disturbance at different levels

An additional experiment with the H-MAN was carried out by the same subject as before in order to explore how our proposed impedance learning method deals with different levels of disturbance in both non-repetitive and repetitive tasks.

Performance and effort were investigated at increasing levels $L = 1, 2, 3, 4, 5$ of disturbance. For the non-repetitive task the disturbance was (with x_1, x_2 in m and $\dot{x}_1, \dot{x}_2$ in m/s) $\boldsymbol{d} = \begin{bmatrix} d_x & d_y \end{bmatrix}^{\mathrm{T}}$ N where $d_x = 8(1+5L)x_1 + 0.4(1+2L)\dot{x}_1$ and $d_y = 8(1+5L)x_2 + 0.4(1+2L)\dot{x}_2$. The disturbance for the repetitive task was with $d_x = 20(1+3L)(\sin 10x_1)^2 x_1 + 8(1+L)(\sin 10x_1)^2\dot{x}_1$ and $d_y = 20(1+3L)(\cos 10x_2)^2 x_2 + 8(1+1L)(\cos 10x_2)^2\dot{x}_2$. Five trials were carried out with each control condition, which were presented in the same pseudo random order as before.

Tracking performance representing the contact stability was analyzed using the *total error*

$$E \equiv \int_0^T \|\boldsymbol{e}(t)\| \, \mathrm{d}t, \tag{29}$$

where T is the non-repetitive task duration or the duration of the last iteration for the repetitive task.

To evaluate the improvement of contact stability and maneuverability, we calculate the decrease of total error and effort with velocity-based adaptation and impedance learning relative to the control off condition, respectively, using

$$P_E = \begin{cases} \frac{E_N - E_{ex}}{E_N} \times 100 & \text{for velocity-based adaptation} \\ \frac{E_N - E_{de}}{E_N} \times 100 & \text{for impedance learning,} \end{cases} \tag{30}$$

$$P_F = \begin{cases} \frac{J_N - J_{ex}}{J_N} \times 100 & \text{for velocity-based adaptation} \\ \frac{J_N - J_{de}}{J_N} \times 100 & \text{for impedance learning,} \end{cases} \tag{31}$$

where E_N, E_{ex} and E_{de} are values of E defined in eq. (29) in the conditions of control off, with the velocity-based adaptation and with the proposed impedance learning method respectively; similarly, J_N, J_{ex} and J_{de} are respectively the values of J (defined in eq. (25) for non-repetitive tasks and eq. (27) for repetitive tasks). According to eqs. (30,31), P_E and P_F indicate the improvement of trajectory tracking accuracy and effort-saving using velocity-based and proposed controls, respectively. The higher value the index is, the

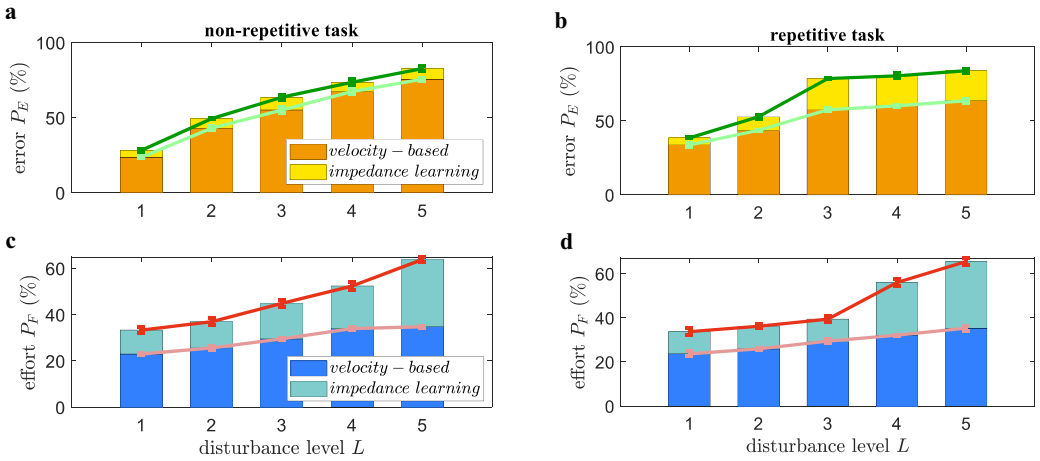

Fig. 6: Relative reduction of total tracking error and effort with disturbances of increasing magnitude (defined in the text) in the non-repetitive task (a) and in the repetitive task (b).

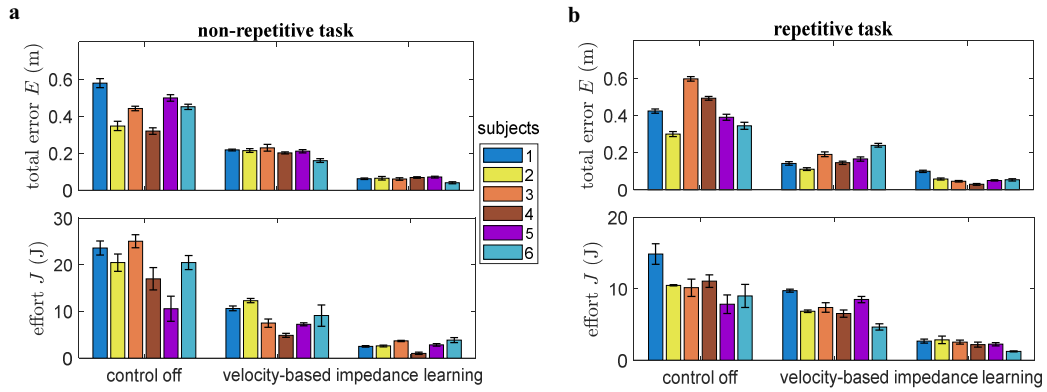

Fig. 7: Results of experiment carried out by six human subjects with the H-MAN robot and different control conditions, to validate the proposed impedance learning on a virtual disturbance. Average and $\pm$ std of total tracking error and effort are over the five trials in the non-repetitive task (a) and in the repetitive task (b) where only the last iteration (of the five trials) is considered.

greater improvement brought by the controller. The parameters of the velocity-based and proposed controllers were maintained as in Sections V.A-B.

Fig. 6 shows the average percentage index P_E and P_F of five trials in different tasks. As we see in Figs. 6a and 6b, impedance learning does not offer an obvious advantage over the velocity-based method to reduce the tracking error for an environmental disturbance of small amplitude. However, in both the non-repetitive and repetitive tasks, the tracking performance benefits increase with the disturbance level, exhibiting less tracking error at higher levels. Due to the limited capability of controllers in improving trajectory tracking performance and the limitation of the robot platform, no further improvement over $L = 3$ is observed in Fig. 6b.

Fig. 6 shows that the effort reduction with both the velocity-based and impedance learning control increases with the disturbance level in the non-repetitive and repetitive tasks. However the benefits of the impedance learning approach are larger compared to the velocity-based approach.

D. Overall results of multiple subjects with H-MAN robot

We can see in Fig. 7 that the proposed control with impedance learning outperforms the velocity-based control in improving the tracking performance and minimizing effort for both non-repetitive and repetitive tasks, which demonstrates its advantages in ensuring the contact stability and maneuverability of the interaction system.

VI. Application to 3D tasks with unknown environment

A second experiment was carried out to test the efficiency of impedance learning control in 3D tasks involving unknown environment's interactions, as well as its robustness to the variability of duration when humans repeat a movement. As shown in Fig. 8a, subjects guided a 7-DoF Franka Emika Panda robot along a reference shape previously traced by the robot while interacting with a cordless rotary carving tool and a grinding tool as shown in Figs. 8c and 8d, respectively. Compared with the software designed disturbance in Section V, the disturbance in this section arises from the contact with the environment due to the hard texture of the environment and the vibration caused by the high-frequency rotation of the

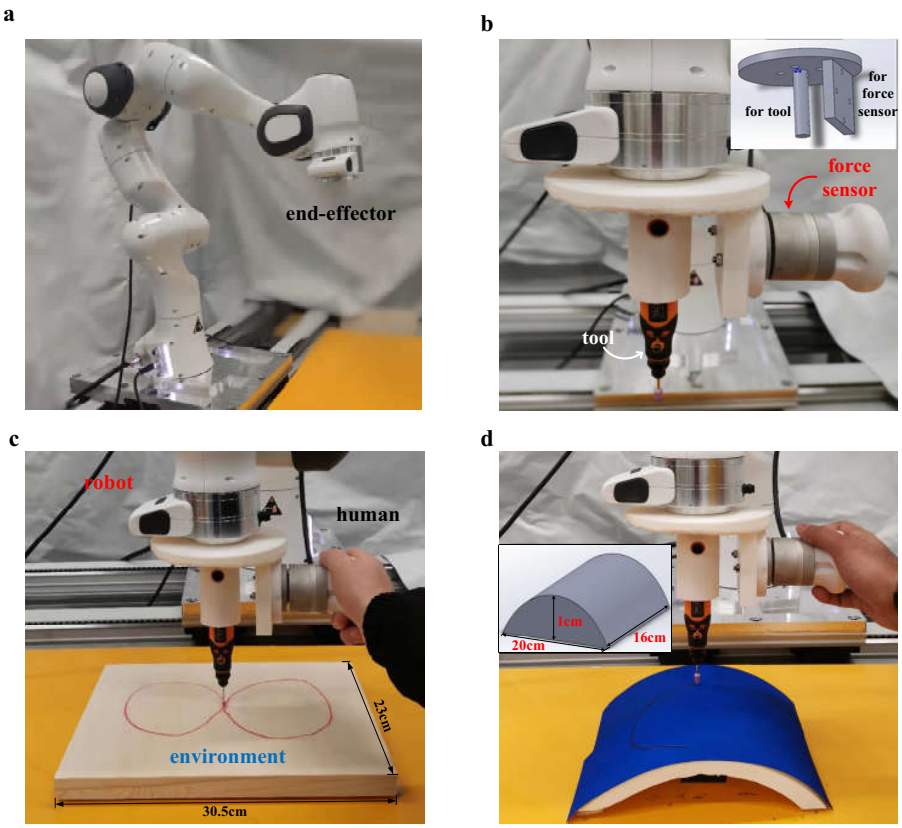

Fig. 8: Experimental setups for 3D tasks in contact with the environment. a: Franka Emika Panda robot with 7-DoFs used in the experiments. b: Mechanism with handle to separate measurement of the user applied interaction force from the interaction with the environment. c: Non-repetitive carving task. d: Repetitive grinding task and the CAD schematic drawing of the 3D surface.

tool. This experiment tests whether the interaction model of eq. (6) is valid in this case and if the controller yields stable and efficient movement assistance to the human operator.

To decouple the human force from the environmental interaction, a mechanism was fixed between the robot extremity and the tool as shown in Fig. 8b. This mechanism was designed to measure the force exerted by the operator and separate it from tool interaction with the environment. The Franka Control Interface (FCI) provides the current status of the robot and an external workstation PC was connected with the Panda robot via Ethernet to realize real-time control at 1 kHz. Joint position and velocity as well as the force exerted on the robot were recorded at 1 kHz.

The experiment protocol was approved by the UWE Research Ethics Committee (UWE REC REF No: FET-2122-59). A total of 12 human subjects without known sensorimotor impairment were recruited to carry out one of the two tasks with the Panda robot (with six subjects for each of them), who gave their informed consent prior to participation. Each subject was allowed to practice until becoming familiar with the robot guidance and the carving or grinding task. They then carried out five trials in each of the conditions control off, velocity-based control in eq. (24) and impedance learning as described in Section V, and were naive to the conditions tested.

Sections VI.A-B show detailed results of a representative, while the overall results of the six subjects are provided in Section VI-C.

A. Non-repetitive carving task

In the non-repetitive carving task, an "8" shape in red colour was first traced by the robot on a hard wooden board with a cordless rotary carving tool as shown in Fig. 8c. Then each subject guided the robot along this shape once for a trial in the three control conditions. Velocity-based adaption was implemented with $a_1 = a_2 = 200$, $b_1 = b_2 = 10$, $c_1 = c_2 = 20$, and impedance learning with $\boldsymbol{K_e} = 150\boldsymbol{I}_2$, $\boldsymbol{A_f} = \boldsymbol{A_d} = \boldsymbol{A_c} = 1000\,\boldsymbol{I}_2$.

The time to carry out the tasks between different trials varies. To be able to compare different trials of a subject and between subjects, the errors in all trials of all subjects were normalised to the average duration of a representative subject.

Fig. 9a shows the character carved by a representative subject in the first trial of the three control conditions. The average norm of the path error $\|e\|$ and the average effort J of the human user defined in eq. (25) of five trials is shown in Fig. 9b and Fig. 9c, respectively. Both the path error and driving effort in the last trial are lowered slightly using the velocity-based control, and reduced more using impedance learning.

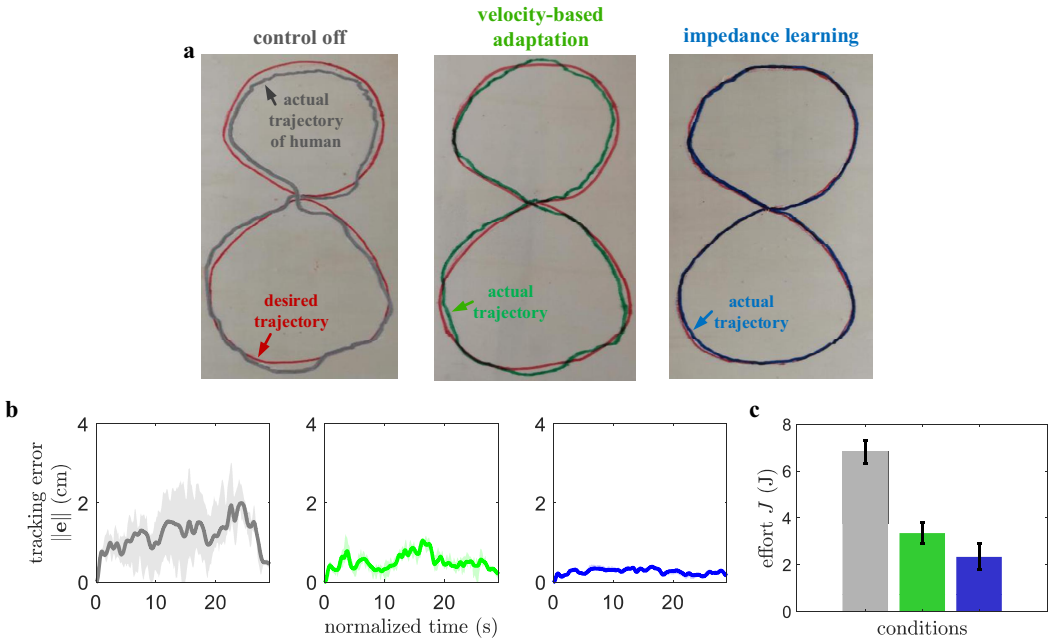

Fig. 9: Results of a representative subject in the non-repetitive carving task with the Panda robot, in control off (grey), with velocity-based control (green), and with the proposed adaptive impedance learning method (blue). a: "8" carved by the human user. b: Average norm of path error with ± std error bars. c: Average effort of the human user with ± std error bars.

B. Repetitive grinding task

In the repetitive grinding task, a cordless rotary tool was mounted on the designed mechanism to grind a rough 3D-printed surface as shown in Fig. 8d. An arc was first traced by the robot on the 3D surface as the reference for the subjects before recording. Then each subject held the force sensor and carried out trials to grind the 3D surface along the reference. Five trials were completed in each condition, where one trial consists of four iterations ($m = 4$ for eqs. (27,28)), i.e. four times back and forth. The parameters were set as $a_1 = a_2 = 200, b_1 = b_2 = 5, c_1 = c_1 = 10$ for the velocity-based adaptation and $\boldsymbol{K_e} = 200\boldsymbol{I}_2$, $\boldsymbol{A} = \boldsymbol{A_v} = 100\,\boldsymbol{I}_2, \boldsymbol{A_p} = 350\,\boldsymbol{I}_2, \eta = 0.001$, $\mu = 0.005$, $\overline{T} = 8\,\mathrm{s}$, $a_1 = a_2 = 200$, $b_1 = b_2 = 5$, $c_1 = c_1 = 10$ for impedance learning.

The results of a representative subject are shown in Fig. 10. We see in the photos of grinding performance of Fig. 10a that all iterations of the first trial deviate from the reference with control off and velocity-based adaptation, without any apparent learning taking place. This bias is caused by the non-negligible robot mechanical impedance experienced when guiding the robot along the 3D surface. To analyze how the tracking performance changes with iterations, the 3D recorded data is reproduced in Fig. 10b, which shows the path from the average of back and forth movements in all iterations. We see that the velocity-based method yields a slight improvement, but performance does not improve over the iterations. With iterative impedance learning, the first iteration similarly deviates from the desired path, but the movement approaches it more with each iteration.

Fig. 10c shows the resulting error and standard deviation error bars as a function of normalized time, in the last iteration over the five trials. The average driving effort in eq. (27) is shown in Fig. 10d. Overall, Fig. 10 exhibits that the velocity-based approach enables limited performance improvement, while impedance learning results in a clear decrease in both path error and the driving effort.

C. Experiment results of multiple subjects for carving and grinding tasks

Figs. 11a and 11b show average values of total path error E defined in eq. (29) and average effort J, respectively over the six subjects that carried out each experiment. We see in Fig. 11 that the velocity-based adaptation algorithm reduces the tracking error and effort relative to control off in two tasks with a limitation as the disturbance can not be fully compensated for. By comparison, the proposed impedance method reduces them more, exhibiting less error and effort than with velocity-based control. These results suggest that impedance learning can handle temporal variability in human movements, and ensure both contact stability and maneuverability in the presence of a real environment.

VII. Discussion

For a human-guided robot, environmental disturbances can result in contact instabilities, requiring the human to increase their control effort at the expense of loss of maneuverability. In this paper, to concurrently ensure contact stability and maneuverability, a novel impedance control scheme was developed. This was first done for non-repetitive tasks, where the robot updates its impedance to adapt to the disturbance with constant coefficients. An iterative impedance control strategy was then designed to handle disturbances with varying space-related coefficients. With the proposed control,

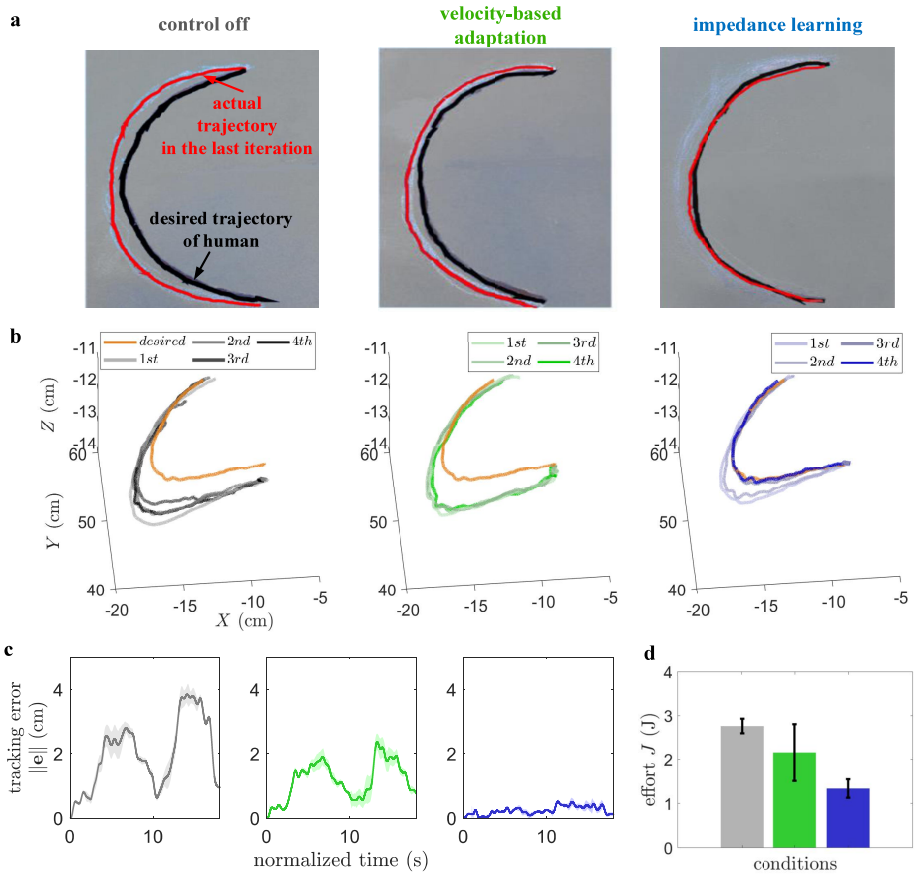

Fig. 10: Results of a representative subject (same subject as Fig. 9) in the repetitive grinding task with the Panda robot. a: Three C-shaped trajectories grinded by the human user. b: Actual trajectories of the human user in the 3D space in four iterations. c: Norm of path errors with $\pm$ std error bars. d: Average effort of the human user with $\pm$ std error bars.

the human effort can be reduced with stable interaction and the robot can follow the desired trajectory in the presence of environmental disturbances. The larger the disturbance, the more obvious the advantage of the proposed strategy. The effectiveness of the proposed impedance control scheme for both non-repetitive and repetitive tasks was validated in experiments to identify a known virtual interaction and to test performance in interaction with real environments.

The experiments also showed that our impedance learning controller outperforms the commonly used velocity-based impedance adaption of [4]. Similar to our method, the velocity-based adaptation method considers both interactions with the human operator and the environment. It infers the human's active intention according to human's velocity, while the robot controller cancels the effect of the environmental disturbance. However, this method does not involve any learning techniques, and the selection of its parameters requires prior knowledge about the task. Namely, the degree of the relationship between the control input and the velocity of the system should be properly reflected when setting the parameters $\boldsymbol{A}' = \mathrm{diag}\{a_j\}$, $\boldsymbol{B}' = \mathrm{diag}\{b_j\}$, $\boldsymbol{C}' = \mathrm{diag}\{c_j\}$. For instance, parameters $\boldsymbol{A}'$ and $\boldsymbol{C}'$ should be selected according to the possible range of velocities of the task so that a variation of the damping within $[\boldsymbol{C}', \boldsymbol{A}']$ can be obtained.

In contrast, the impedance learning controller introduced in this paper uses an explicit model of the environment interaction. As a consequence, it does not require prior knowledge of the environment to guarantee the stability of the system, as was proved in the appendices and verified in the experiments carried out in real environments.

The proposed controller may be extended to teleoperation, where impedance learning can ensure the contact stability between the remote robot and its environment, while no additional control effort is required from the human operator. The learning capability of the proposed controller may play a more significant role where time delay exists in the teleoperation system. In this case, even if the human operator makes more control effort, they may still fail to handle the contact between the robot and the environment. One of our future works will be investigation of this hypothesis.

Appendix 1: Proof of Theorem 1

This Appendix describes the proof of Theorem 1 in Section III. To attenuate the undesired effect of the unknown environment during trajectory tracking, both tracking error and estimation errors are minimized. We therefore introduce

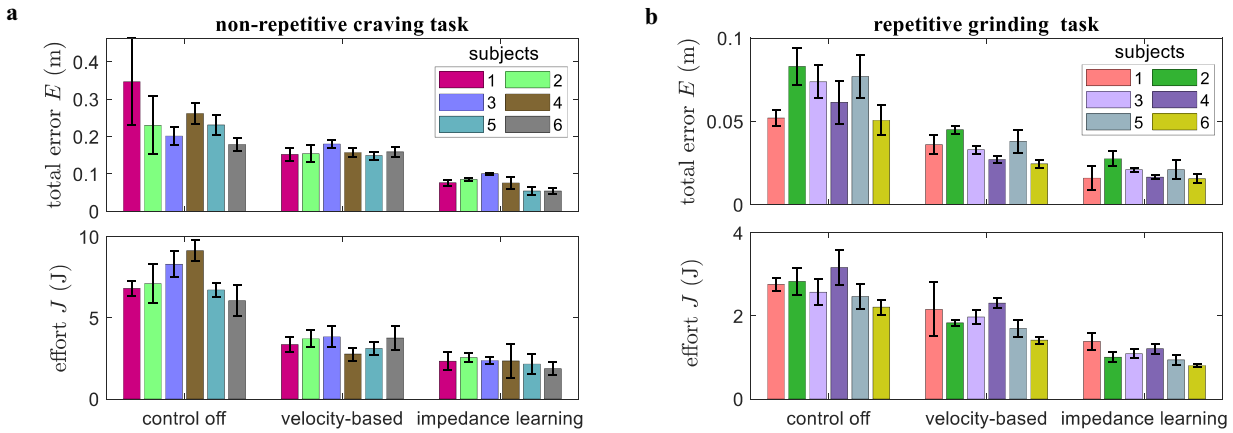

Fig. 11: Total error and effort of six subjects in the carving and grinding tasks carried out on the Panda robot with control off, velocity-based adaptation and impedance learning. Each column shows the average and $\pm$ std error bars.

the Lyapunov function candidate

$$
\begin{aligned}
&V = V_1 + V_2 + V_3 + V_4\,,\\
&V_1 = \frac{1}{2}\dot{\boldsymbol{e}}^{\mathrm{T}}\boldsymbol{M}\,\dot{\boldsymbol{e}}\,, \quad V_2 = \frac{1}{2}\sum_{j=1}^{n}\frac{1}{A_f^j}\left(\tilde{\boldsymbol{k}}^j\right)^{\mathrm{T}}\tilde{\boldsymbol{k}}^j\,, \qquad (32)\\
&V_3 = \frac{1}{2}\sum_{j=1}^{n}\frac{1}{A_d^j}\left(\tilde{\boldsymbol{k}}_{\boldsymbol{v}}^j\right)^{\mathrm{T}}\tilde{\boldsymbol{k}}_{\boldsymbol{v}}^j\,, \quad V_4 = \frac{1}{2}\sum_{j=1}^{n}\frac{1}{A_c^j}\left(\tilde{k}_p^j\right)^2,
\end{aligned}
$$

where V_1 is a quadratic function of the robot tracking error, and V_2, V_3, V_4 denote the squared estimation errors of disturbance coefficients; $\tilde{\boldsymbol{k}}^j$, $\tilde{\boldsymbol{k}}_{\boldsymbol{v}}^j \in \mathbb{R}^n$ are respectively the jth column vectors of $\mathbb{R}^{n\times n}$ matrices $\tilde{\boldsymbol{K}}$ and $\tilde{\boldsymbol{K}}_{\boldsymbol{v}}$, where $j = 1, 2, \cdots, n$; $\tilde{k}_p^j \in \mathbb{R}$ is the jth element of $\mathbb{R}^n$ vector $\tilde{\boldsymbol{k}}_{\boldsymbol{p}}$ in eq. (18); positive constants A_f^j, A_d^j, $A_c^j \in \mathbb{R}$ are the jth diagonal elements of $\mathbb{R}^{n\times n}$ matrices $\boldsymbol{A_f}$, $\boldsymbol{A_d}$, $\boldsymbol{A_c}$, respectively.

Using eq. (17) and the skew-symmetry property, i.e., $\boldsymbol{\zeta}^{\mathrm{T}}(\frac{1}{2}\dot{\boldsymbol{M}} - \boldsymbol{B})\boldsymbol{\zeta} = 0$ for $\forall \boldsymbol{\zeta} \in \mathbb{R}^n$, the derivative of V_1 is

$$
\dot{V}_1 = \dot{\boldsymbol{e}}^{\mathrm{T}}\left(-\boldsymbol{K_e}\,\dot{\boldsymbol{e}} + \tilde{\boldsymbol{K}}\boldsymbol{x} + \tilde{\boldsymbol{K}}_{\boldsymbol{v}}\,\dot{\boldsymbol{x}} + \tilde{\boldsymbol{k}}_{\boldsymbol{p}}\right). \qquad (33)
$$

Taking the derivatives of V_2, V_3, V_4 and using eq. (12) yields

$$
\begin{aligned}
\dot{V}_2 &= -\sum_{j=1}^{n}\frac{1}{A_f^j}\left(\tilde{\boldsymbol{k}}^j\right)^{\mathrm{T}}\dot{\hat{\boldsymbol{k}}}^j = -\sum_{j=1}^{n}\left(\tilde{\boldsymbol{k}}^j\right)^{\mathrm{T}}\dot{\boldsymbol{e}}\,x_j, \qquad (34)\\
\dot{V}_3 &= -\sum_{j=1}^{n}\frac{1}{A_d^j}\left(\tilde{\boldsymbol{k}}_{\boldsymbol{v}}^j\right)^{\mathrm{T}}\dot{\hat{\boldsymbol{k}}}_{\boldsymbol{v}}^j = -\sum_{j=1}^{n}\left(\tilde{\boldsymbol{k}}_{\boldsymbol{v}}^j\right)^{\mathrm{T}}\dot{\boldsymbol{e}}\,\dot{x}_j, \qquad (35)\\
\dot{V}_4 &= -\sum_{j=1}^{n}\frac{1}{A_c^j}\tilde{k}_p^j\dot{\hat{k}}_p^j = -\sum_{j=1}^{n}\tilde{k}_p^j\,\dot{e}_j\,. \qquad (36)
\end{aligned}
$$

where $\hat{\boldsymbol{k}}^j$, $\hat{\boldsymbol{k}}_{\boldsymbol{v}}^j \in \mathbb{R}^n$ are the jth column vectors of $\mathbb{R}^{n\times n}$ matrices $\hat{\boldsymbol{K}}$ and $\hat{\boldsymbol{K}}_{\boldsymbol{v}}$, and $\hat{k}_p^j$, x_j, $e_j \in \mathbb{R}$ are the jth elements of $\mathbb{R}^n$ vectors $\hat{\boldsymbol{k}}_{\boldsymbol{p}}$, $\boldsymbol{x}$ and $\boldsymbol{e}$.

Then $\dot{V}$ can be computed by summing up eqs. (33-36) as

$$
\begin{aligned}
\dot{V} &= \dot{V}_1 + \dot{V}_2 + \dot{V}_3 + \dot{V}_4\\
&= \dot{\boldsymbol{e}}^{\mathrm{T}}\left(-\boldsymbol{K_e}\,\dot{\boldsymbol{e}} + \tilde{\boldsymbol{K}}\boldsymbol{x} + \tilde{\boldsymbol{K}}_{\boldsymbol{v}}\dot{\boldsymbol{x}} + \tilde{\boldsymbol{k}}_{\boldsymbol{p}}\right) - \sum_{j=1}^{n}\tilde{k}_p^j\,\dot{e}_j\\
&\quad - \sum_{j=1}^{n}\left(\tilde{\boldsymbol{k}}^j\right)^{\mathrm{T}}\dot{\boldsymbol{e}}x_j - \sum_{j=1}^{n}\left(\tilde{\boldsymbol{k}}_{\boldsymbol{v}}^j\right)^{\mathrm{T}}\dot{\boldsymbol{e}}\dot{x}_j \qquad (37)\\
&= -\dot{\boldsymbol{e}}^{\mathrm{T}}\boldsymbol{K_e}\,\dot{\boldsymbol{e}} \le 0,
\end{aligned}
$$

where the term $\dot{\boldsymbol{e}}^{\mathrm{T}}\tilde{\boldsymbol{K}}\boldsymbol{x}$ is cancelled by $-\sum_{j=1}^{n}\left(\tilde{\boldsymbol{k}}^j\right)^{\mathrm{T}}\dot{\boldsymbol{e}}x_j$, $\dot{\boldsymbol{e}}^{\mathrm{T}}\tilde{\boldsymbol{K}}_{\boldsymbol{v}}\dot{\boldsymbol{x}}$ by $-\sum_{j=1}^{n}\left(\tilde{\boldsymbol{k}}_{\boldsymbol{v}}^j\right)^{\mathrm{T}}\dot{\boldsymbol{e}}\dot{x}_j$, and $\dot{\boldsymbol{e}}^{\mathrm{T}}\tilde{\boldsymbol{k}}_{\boldsymbol{p}}$ by $-\sum_{j=1}^{n}\tilde{k}_p^j\dot{e}_j$.

Applying Lemma A.6 in [29], it then follows

$$
\lim_{t\to\infty}\dot{\boldsymbol{e}} = \lim_{t\to\infty}\ddot{\boldsymbol{e}} = 0 \qquad (38)
$$

and with eq. (17)

$$
\lim_{t\to\infty}\left(\tilde{\boldsymbol{K}}\boldsymbol{x} + \tilde{\boldsymbol{K}}_{\boldsymbol{v}}\,\dot{\boldsymbol{x}} + \tilde{\boldsymbol{k}}_{\boldsymbol{p}}\right) = 0 \qquad (39)
$$

so that the environmental disturbance can be estimated and the human can easily guide the robot even with the disturbance of an unknown environment.

Appendix 2: Proof of Theorem 2

In the space domain, the robot controller in eq. (20) can be rewritten as follows

$$
\boldsymbol{u}_i = -\hat{\boldsymbol{K}}_{\boldsymbol{s},i}\,\boldsymbol{x}_i - \hat{\boldsymbol{K}}_{\boldsymbol{vs},i}\,\dot{\boldsymbol{x}}_i - \hat{\boldsymbol{k}}_{\boldsymbol{ps},i} - \boldsymbol{K_e}\dot{\boldsymbol{e}}_i + \boldsymbol{g}\,, \qquad (40)
$$

where space-related impedance matrices $\hat{\boldsymbol{K}}_{\boldsymbol{s},i} \in \mathbb{R}^{n\times n}$ and $\hat{\boldsymbol{K}}_{\boldsymbol{vs},i} \in \mathbb{R}^{n\times n}$ and vector $\hat{\boldsymbol{k}}_{\boldsymbol{ps},i} \in \mathbb{R}^n$ should be updated with the position change of the robot.

The undesired effect of the unknown environment is expected to be cancelled by the robot during trajectory tracking, which is both to minimise the tracking error and improve the environment identification. Consequently, a Lyapunov function candidate is designed as follows to prove the stability of the controlled human-guided robot in Section IV

$$
V_i = V_{e,i} + V_{k,i} + V_{v,i} + V_{p,i}\,,
$$

$$V_{e,i}=\frac{1}{2}\dot{\boldsymbol{e}}_i^T\boldsymbol{M}\,\dot{\boldsymbol{e}}_i\,,\quad V_{k,i}=\frac{1}{2}\int_\Omega \boldsymbol{\Psi}_{\boldsymbol{ks},i}\left(\boldsymbol{\xi}\right)\mathrm{d}\boldsymbol{\xi}\,,$$

$$V_{v,i}=\frac{1}{2}\int_\Omega \boldsymbol{\Psi}_{\boldsymbol{vs},i}\left(\boldsymbol{\xi}\right)\,\mathrm{d}\boldsymbol{\xi}\,,\quad V_{p,i}=\frac{1}{2}\int_\Omega \boldsymbol{\Psi}_{\boldsymbol{ps},i}\left(\boldsymbol{\xi}\right)\mathrm{d}\boldsymbol{\xi}\,,$$

$$\boldsymbol{\varepsilon}_i=\begin{cases}\boldsymbol{e}_i\,,\ \text{if } t\in[0,T_i]\\ \boldsymbol{e}_i\left(T_i\right),\ \text{if } t\in\left(T_i,\overline{T}\right]\end{cases},$$

$$\boldsymbol{\xi}=\begin{bmatrix}\xi^1 & \cdots & \xi^n\end{bmatrix},\quad \mathrm{d}\boldsymbol{\xi}=\begin{bmatrix}\mathrm{d}\xi^1 & \cdots & \mathrm{d}\xi^n\end{bmatrix},$$

$$\begin{aligned}\boldsymbol{\Psi}_{\boldsymbol{ks},i}\left(\boldsymbol{\xi}\right)=\Bigg[&\tfrac{1}{\alpha^1}\left(\tilde{\boldsymbol{k}}^1_{\boldsymbol{s},i}\left(\boldsymbol{\xi}\right)\right)^{\mathrm{T}}\operatorname{sgn}\left(v^1\right)\tilde{\boldsymbol{k}}^1_{\boldsymbol{s},i}\left(\boldsymbol{\xi}\right)\quad\cdots\\ &\frac{1}{\alpha^n}\left(\tilde{\boldsymbol{k}}^n_{\boldsymbol{s},i}\left(\boldsymbol{\xi}\right)\right)^{\mathrm{T}}\operatorname{sgn}\left(v^n\right)\tilde{\boldsymbol{k}}^n_{\boldsymbol{s},i}\left(\boldsymbol{\xi}\right)\Bigg],\end{aligned}$$

$$\begin{aligned}\boldsymbol{\Psi}_{\boldsymbol{vs},i}\left(\boldsymbol{\xi}\right)=\Bigg[&\tfrac{1}{\alpha_v^1}\left(\tilde{\boldsymbol{k}}^1_{\boldsymbol{vs},i}\left(\boldsymbol{\xi}\right)\right)^{\mathrm{T}}\operatorname{sgn}\left(v^1\right)\tilde{\boldsymbol{k}}^1_{\boldsymbol{vs},i}\left(\boldsymbol{\xi}\right)\quad\cdots\\ &\frac{1}{\alpha_v^n}\left(\tilde{\boldsymbol{k}}^n_{\boldsymbol{vs},i}\left(\boldsymbol{\xi}\right)\right)^{\mathrm{T}}\operatorname{sgn}\left(v^n\right)\tilde{\boldsymbol{k}}^n_{\boldsymbol{vs},i}\left(\boldsymbol{\xi}\right)\Bigg],\end{aligned}$$

$$\begin{aligned}\boldsymbol{\Psi}_{\boldsymbol{ps},i}\left(\boldsymbol{\xi}\right)=\Bigg[&\tfrac{1}{\alpha_p^1}\operatorname{sgn}\left(v^1\right)\left(\tilde{k}^1_{ps,i}\left(\boldsymbol{\xi}\right)\right)^2\quad\cdots\\ &\frac{1}{\alpha_p^n}\operatorname{sgn}\left(v^n\right)\left(\tilde{k}^n_{ps,i}\left(\boldsymbol{\xi}\right)\right)^2\Bigg],\end{aligned}\tag{41}$$

where $V_{e,i}$ denotes the robot tracking error; $V_{k,i}$, $V_{v,i}$ and $V_{p,i}$ are estimation errors of the coefficients of the disturbance represented by the introduced Ψ functions; $\Omega=\{x,0\le t\le\overline{T}\}$; $\tilde{\boldsymbol{k}}^j_{\boldsymbol{s},i}\in\mathbb{R}^n$ and $\tilde{\boldsymbol{k}}^j_{\boldsymbol{vs},i}\in\mathbb{R}^n$ are the jth column vectors of $\mathbb{R}^{n\times n}$ matrices $\tilde{\boldsymbol{K}}_{\boldsymbol{s},i}=\boldsymbol{K}_{\boldsymbol{s}}-\hat{\boldsymbol{K}}_{\boldsymbol{s},i}$ and $\tilde{\boldsymbol{K}}_{\boldsymbol{vs},i}=\boldsymbol{K}_{\boldsymbol{vs}}-\hat{\boldsymbol{K}}_{\boldsymbol{vs},i}$, respectively; $\tilde{k}^j_{ps,i}\in\mathbb{R}$ is the jth element of $\mathbb{R}^n$ vector $\tilde{\boldsymbol{k}}_{\boldsymbol{ps},i}=\boldsymbol{k}_{\boldsymbol{ps}}-\hat{\boldsymbol{k}}_{\boldsymbol{ps},i}$; $\operatorname{sgn}(\cdot)$ is the sign function; positive constants α^j, α_v^j, $\alpha_p^j\in\mathbb{R}$ are the the jth diagonal elements of $\mathbb{R}^{n\times n}$ matrices $\boldsymbol{A}$, $\boldsymbol{A_v}$, $\boldsymbol{A_p}$, respectively. Since the stability of the iterative learning control is verified from the perspective of iterations instead of time, $V_{k,i}$, $V_{v,i}$ and $V_{p,i}$ are respectively designed to be in an integral form of functions $\boldsymbol{\Psi}_{\boldsymbol{ks},i}$, $\boldsymbol{\Psi}_{\boldsymbol{vs},i}$ and $\boldsymbol{\Psi}_{\boldsymbol{ps},i}$ in one iteration.

Since

$$\begin{aligned}V_{k,i}=&\frac{1}{2}\sum_{j=1}^n\int_0^{s^j}\frac{1}{\alpha^j}\left(\tilde{\boldsymbol{k}}^j_{\boldsymbol{s},i}\right)^{\mathrm{T}}\operatorname{sgn}\left(v^j\right)\tilde{\boldsymbol{k}}^j_{\boldsymbol{s},i}\,\mathrm{d}\xi^j\\ =&\frac{1}{2}\sum_{j=1}^n\int_0^{t}\frac{1}{\alpha^j}\left(\tilde{\boldsymbol{k}}^j_{\boldsymbol{s},i}\right)^{\mathrm{T}}\operatorname{sgn}\left(v^j\right)\tilde{\boldsymbol{k}}^j_{\boldsymbol{s},i}\,\dot{\xi}^j\,\mathrm{d}\sigma\\ =&\frac{1}{2}\sum_{j=1}^n\int_0^{t}\frac{1}{\alpha^j}\left(\tilde{\boldsymbol{k}}^j_{\boldsymbol{s},i}\right)^{\mathrm{T}}\left|v^j\right|\tilde{\boldsymbol{k}}^j_{\boldsymbol{s},i}\,\mathrm{d}\sigma>0\end{aligned}\tag{42}$$

and similarly

$$V_{v,i}=\frac{1}{2}\sum_{j=1}^n\int_0^{t}\frac{1}{\alpha_v^j}\left(\tilde{\boldsymbol{k}}^j_{\boldsymbol{vs},i}\right)^{\mathrm{T}}\left|v^j\right|\tilde{\boldsymbol{k}}^j_{\boldsymbol{vs},i}\,\mathrm{d}\sigma>0\,,\tag{43}$$

$$V_{p,i}=\frac{1}{2}\sum_{j=1}^n\int_0^{t}\frac{1}{\alpha_p^j}\left|v^j\right|\left(\tilde{k}^j_{ps,i}\right)^2\mathrm{d}\sigma>0\,,\tag{44}$$

where σ is an integration variable of time, the system Lyapunov function in eq. (41) is positive and satisfies $V_i>0$.

The following cases are considered for stability analysis:

Case 1: $t\in[0,T_i]$. In such a case, $\boldsymbol{\varepsilon}_i=\boldsymbol{e}_i$ holds and taking the derivative of $V_{e,i}$ yields

$$\dot{V}_{e,i}=\dot{\boldsymbol{e}}_i^{\mathrm{T}}\boldsymbol{M}\ddot{\boldsymbol{e}}_i+\frac{1}{2}\dot{\boldsymbol{e}}_i^{\mathrm{T}}\dot{\boldsymbol{M}}\dot{\boldsymbol{e}}_i\tag{45}$$

Based on the skew-symmetry property [25], substituting eq. (22) into eq. (45) yields

$$\dot{V}_{e,i}=\dot{\boldsymbol{e}}_i^{\mathrm{T}}\left(-\boldsymbol{K_e}\,\dot{\boldsymbol{e}}_i+\tilde{\boldsymbol{K}}_i\,\boldsymbol{x}_i+\tilde{\boldsymbol{K}}_{\boldsymbol{v},i}\,\dot{\boldsymbol{x}}_i+\tilde{\boldsymbol{k}}_{\boldsymbol{p},i}\right).\tag{46}$$

The integral of eq. (46) can be calculated as

$$\begin{aligned}V_{e,i}=&\int_0^t\dot{V}_{e,i}\,\mathrm{d}\sigma+V_{e,i}\left(0\right)\\ =&\int_0^t\dot{\boldsymbol{e}}_i^{\mathrm{T}}\left(-\boldsymbol{K_e}\,\dot{\boldsymbol{e}}_i+\tilde{\boldsymbol{K}}_i\,\boldsymbol{x}_i+\tilde{\boldsymbol{K}}_{\boldsymbol{v},i}\,\dot{\boldsymbol{x}}_i+\tilde{\boldsymbol{k}}_{\boldsymbol{p},i}\right)\mathrm{d}\sigma\,.\end{aligned}\tag{47}$$

Define

$$\Delta V_{e,i}=V_{e,i}-V_{e,i-1}\tag{48}$$

and then we have

$$\Delta V_{e,i}\le\int_0^t\dot{\boldsymbol{e}}_i^{\mathrm{T}}\left(-\boldsymbol{K_e}\dot{\boldsymbol{e}}_i+\tilde{\boldsymbol{K}}_i\,\boldsymbol{x}_i+\tilde{\boldsymbol{K}}_{\boldsymbol{v},i}\,\dot{\boldsymbol{x}}_i+\tilde{\boldsymbol{k}}_{\boldsymbol{p},i}\right)\mathrm{d}\sigma\,.\tag{49}$$

Similarly, we define

$$\Delta V_{k,i}=V_{k,i}-V_{k,i-1},\tag{50}$$

$$\Delta V_{v,i}=V_{v,i}-V_{v,i-1},\tag{51}$$

$$\Delta V_{p,i}=V_{p,i}-V_{p,i-1}.\tag{52}$$

Then according to eq. (42), we get

$$\begin{aligned}\Delta V_{k,i}=&\frac{1}{2}\sum_{j=1}^n\frac{1}{\alpha^j}\int_0^{s^j}\Bigg[\left(\tilde{\boldsymbol{k}}^j_{\boldsymbol{s},i}\right)^{\mathrm{T}}\operatorname{sgn}\left(v^j\right)\tilde{\boldsymbol{k}}^j_{\boldsymbol{s},i}\\ &-\left(\tilde{\boldsymbol{k}}^j_{\boldsymbol{s},i}\right)^{\mathrm{T}}\operatorname{sgn}\left(v^j\right)\tilde{\boldsymbol{k}}^j_{\boldsymbol{s},i-1}+\left(\tilde{\boldsymbol{k}}^j_{\boldsymbol{s},i}\right)^{\mathrm{T}}\operatorname{sgn}\left(v^j\right)\tilde{\boldsymbol{k}}^j_{\boldsymbol{s},i-1}\\ &-\left(\tilde{\boldsymbol{k}}^j_{\boldsymbol{s},i-1}\right)^{\mathrm{T}}\operatorname{sgn}\left(v^j\right)\tilde{\boldsymbol{k}}^j_{\boldsymbol{s},i-1}\Bigg]\mathrm{d}\xi^j.\end{aligned}\tag{53}$$

Define

$$\Delta\hat{\boldsymbol{K}}_{\boldsymbol{s},i}\left(\boldsymbol{\xi}\right)=\hat{\boldsymbol{K}}_{\boldsymbol{s},i}\left(\boldsymbol{\xi}\right)-\hat{\boldsymbol{K}}_{\boldsymbol{s},i-1}\left(\boldsymbol{\xi}\right),\tag{54}$$

$$\Delta\hat{\boldsymbol{K}}_{\boldsymbol{vs},i}\left(\boldsymbol{\xi}\right)=\hat{\boldsymbol{K}}_{\boldsymbol{vs},i}\left(\boldsymbol{\xi}\right)-\hat{\boldsymbol{K}}_{\boldsymbol{vs},i-1}\left(\boldsymbol{\xi}\right),\tag{55}$$

$$\Delta\hat{\boldsymbol{k}}_{\boldsymbol{ps},i}\left(\boldsymbol{\xi}\right)=\hat{\boldsymbol{k}}_{\boldsymbol{ps},i}\left(\boldsymbol{\xi}\right)-\hat{\boldsymbol{k}}_{\boldsymbol{ps},i-1}\left(\boldsymbol{\xi}\right),\tag{56}$$

and thus we have

$$\tilde{\boldsymbol{K}}_{\boldsymbol{s},i}\left(\boldsymbol{\xi}\right)-\tilde{\boldsymbol{K}}_{\boldsymbol{s},i-1}\left(\boldsymbol{\xi}\right)=-\Delta\hat{\boldsymbol{K}}_{\boldsymbol{s},i}\left(\boldsymbol{\xi}\right),\tag{57}$$

$$\tilde{\boldsymbol{K}}_{\boldsymbol{vs},i}\left(\boldsymbol{\xi}\right)-\tilde{\boldsymbol{K}}_{\boldsymbol{vs},i-1}\left(\boldsymbol{\xi}\right)=-\Delta\hat{\boldsymbol{K}}_{\boldsymbol{vs},i}\left(\boldsymbol{\xi}\right),\tag{58}$$

$$\tilde{\boldsymbol{k}}_{\boldsymbol{ps},i}\left(\boldsymbol{\xi}\right)-\tilde{\boldsymbol{k}}_{\boldsymbol{ps},i-1}\left(\boldsymbol{\xi}\right)=-\Delta\hat{\boldsymbol{k}}_{\boldsymbol{ps},i}\left(\boldsymbol{\xi}\right).\tag{59}$$

Using eq. (57), eq. (53) can be rewritten as

$$\begin{aligned}\Delta V_{k,i} &= -\frac{1}{2}\sum_{j=1}^{n}\frac{1}{\alpha^j}\int_0^{s^j}\Big[\Big(\tilde{\boldsymbol{k}}_{\boldsymbol{s},i}^j\Big)^{\mathrm{T}}\operatorname{sgn}\left(v^j\right)\Delta\hat{\boldsymbol{k}}_{\boldsymbol{s},i}^j \\ &\quad+\Big(\tilde{\boldsymbol{k}}_{\boldsymbol{s},i-1}^j\Big)^{\mathrm{T}}\operatorname{sgn}\left(v^j\right)\Delta\hat{\boldsymbol{k}}_{\boldsymbol{s},i}^j\Big]\,\mathrm{d}\xi^j \\ &= -\sum_{j=1}^{n}\frac{1}{\alpha^j}\int_0^{s^j}\left(\tilde{\boldsymbol{k}}_{\boldsymbol{s},i}^j+\frac{1}{2}\Delta\hat{\boldsymbol{k}}_{\boldsymbol{s},i}^j\right)^{\mathrm{T}}\operatorname{sgn}\left(v^j\right)\Delta\hat{\boldsymbol{k}}_{\boldsymbol{s},i}^j\,\mathrm{d}\xi^j\end{aligned} \tag{60}$$

and thus one gets

$$\Delta V_{k,i}\le-\sum_{j=1}^{n}\frac{1}{\alpha^j}\int_0^t\Big(\tilde{\boldsymbol{k}}_i^j\Big)^{\mathrm{T}}\left|v^j\right|\Delta\hat{\boldsymbol{k}}_i^j\,\mathrm{d}\sigma\,. \tag{61}$$

Similarly, using eqs. (43,58) and eqs. (44,59) yields

$$\Delta V_{v,i}\le-\sum_{j=1}^{n}\frac{1}{\alpha_v^j}\int_0^t\Big(\tilde{\boldsymbol{k}}_{\boldsymbol{v},i}^j\Big)^{\mathrm{T}}\left|v^j\right|\Delta\hat{\boldsymbol{k}}_{\boldsymbol{v},i}^j\,\mathrm{d}\sigma, \tag{62}$$

$$\Delta V_{p,i}\le-\sum_{j=1}^{n}\frac{1}{\alpha_p^j}\int_0^t\tilde{k}_{p,i}^j\left|v^j\right|\Delta\hat{k}_{p,i}^j\,\mathrm{d}\sigma\,. \tag{63}$$

Summing up inequalities (49,61,62,63) yields

$$\begin{aligned}\Delta V_i &\le \int_0^t\dot{\boldsymbol{e}}_i^{\mathrm{T}}\left(-\boldsymbol{K}_{\boldsymbol{e}}\,\dot{\boldsymbol{e}}_i+\tilde{\boldsymbol{K}}_i\,\boldsymbol{x}_i+\tilde{\boldsymbol{K}}_{\boldsymbol{v},i}\,\dot{\boldsymbol{x}}_i+\tilde{\boldsymbol{k}}_{\boldsymbol{p},i}\right)\mathrm{d}\sigma \\ &\quad-\sum_{j=1}^{n}\frac{1}{\alpha^j}\int_0^t\Big(\tilde{\boldsymbol{k}}_i^j\Big)^{\mathrm{T}}\left|v^j\right|\Delta\hat{\boldsymbol{k}}_i^j\,\mathrm{d}\sigma \\ &\quad-\sum_{j=1}^{n}\frac{1}{\alpha_v^j}\int_0^t\Big(\tilde{\boldsymbol{k}}_{\boldsymbol{v},i}^j\Big)^{\mathrm{T}}\left|v^j\right|\Delta\hat{\boldsymbol{k}}_{\boldsymbol{v},i}^j\,\mathrm{d}\sigma \\ &\quad-\sum_{j=1}^{n}\frac{1}{\alpha_p^j}\int_0^t\tilde{k}_{p,i}^j\left|v^j\right|\Delta\hat{k}_{p,i}^j\,\mathrm{d}\sigma.\end{aligned} \tag{64}$$

Substituting eq. (21) into inequality (64), we have

$$\begin{aligned}\Delta V_i &\le \int_0^t\dot{\boldsymbol{e}}_i^{\mathrm{T}}\left(-\boldsymbol{K}_{\boldsymbol{e}}\,\dot{\boldsymbol{e}}_i+\tilde{\boldsymbol{K}}_i\,\boldsymbol{x}_i+\tilde{\boldsymbol{K}}_{\boldsymbol{v},i}\,\dot{\boldsymbol{x}}_i+\tilde{\boldsymbol{k}}_{\boldsymbol{p},i}\right)\mathrm{d}\sigma \\ &\quad-\sum_{j=1}^{n}\int_0^t\tilde{k}_{p,i}^j\dot{e}_i^j\,\mathrm{d}\sigma-\sum_{j=1}^{n}\int_0^t\Big(\tilde{\boldsymbol{k}}_i^j\Big)^{\mathrm{T}}\dot{\boldsymbol{e}}_i\,x_i^j\,\mathrm{d}\sigma \\ &\quad-\sum_{j=1}^{n}\int_0^t\Big(\tilde{\boldsymbol{k}}_{\boldsymbol{v},i}^j\Big)^{\mathrm{T}}\dot{\boldsymbol{e}}_i\,\dot{x}_i^j\,\mathrm{d}\sigma \\ &= -\int_0^t\dot{\boldsymbol{e}}_i^T\boldsymbol{K}_{\boldsymbol{e}}\,\dot{\boldsymbol{e}}_i\,\mathrm{d}\sigma\le 0,\end{aligned} \tag{65}$$

where $e_i^j\in\mathbb{R}$ and $x_i^j\in\mathbb{R}$ are the jth elements of $\boldsymbol{e}_i\in\mathbb{R}^n$ and $\boldsymbol{x}_i\in\mathbb{R}^n$, respectively.

Case 2: $t\in(T_i,\overline{T}\,]$. According to the definition of $\boldsymbol{\varepsilon}_i$ and eqs. (47,48), one gets

$$\begin{aligned}\Delta V_{e,i} &\le V_{e,i}\left(t\right) \\ &= \int_0^{T_i}\dot{\boldsymbol{e}}_i^{\mathrm{T}}\left(-\boldsymbol{K}_{\boldsymbol{e}}\,\dot{\boldsymbol{e}}_i+\tilde{\boldsymbol{K}}_i\,\boldsymbol{x}_i+\tilde{\boldsymbol{K}}_{\boldsymbol{v},i}\,\dot{\boldsymbol{x}}_i+\tilde{\boldsymbol{k}}_{\boldsymbol{p},i}\right)\mathrm{d}\sigma.\end{aligned} \tag{66}$$

Observing eq. (21), it is known that $\hat{\boldsymbol{K}}_i$, $\hat{\boldsymbol{K}}_{\boldsymbol{v},i}$, and $\hat{\boldsymbol{k}}_{\boldsymbol{p},i}$ stop updating during $t\in(T_i,\overline{T}\,]$ so that $\Delta\hat{\boldsymbol{K}}_i=\Delta\hat{\boldsymbol{K}}_{\boldsymbol{v},i}=\Delta\hat{\boldsymbol{k}}_{\boldsymbol{p},i}=\boldsymbol{0}$. Then according to eqs. (61-63), the following inequality holds

$$\begin{aligned}&\Delta V_{k,i}+\Delta V_{v,i}+\Delta V_{p,i} \\ &\le-\sum_{j=1}^{n}\frac{1}{\alpha^j}\int_0^{T_i}\Big(\tilde{\boldsymbol{k}}_i^j\Big)^{\mathrm{T}}\left|v^j\right|\Delta\hat{\boldsymbol{k}}_i^j\,\mathrm{d}\sigma \\ &\quad-\sum_{j=1}^{n}\frac{1}{\alpha_v^j}\int_0^{T_i}\Big(\tilde{\boldsymbol{k}}_{\boldsymbol{v},i}^j\Big)^{\mathrm{T}}\left|v^j\right|\Delta\hat{\boldsymbol{k}}_{\boldsymbol{v},i}^j\,\mathrm{d}\sigma \\ &\quad-\sum_{j=1}^{n}\frac{1}{\alpha_p^j}\int_0^{T_i}\tilde{k}_{p,i}^j\left|v^j\right|\Delta\hat{k}_{p,i}^j\,\mathrm{d}\sigma.\end{aligned} \tag{67}$$

Combing inequalities (66,67), we have

$$\begin{aligned}\Delta V_i &= \Delta V_{e,i}+\Delta V_{k,i}+\Delta V_{v,i}+\Delta V_{p,i} \\ &\le\int_0^{T_i}\dot{\boldsymbol{e}}_i^{\mathrm{T}}\left(-\boldsymbol{K}_{\boldsymbol{e}}\,\dot{\boldsymbol{e}}_i+\tilde{\boldsymbol{K}}_i\,\boldsymbol{x}_i+\tilde{\boldsymbol{K}}_{\boldsymbol{v},i}\,\dot{\boldsymbol{x}}_i+\tilde{\boldsymbol{k}}_{\boldsymbol{p},i}\right)\mathrm{d}\sigma \\ &\quad-\sum_{j=1}^{n}\frac{1}{\alpha^j}\int_0^{T_i}\Big(\tilde{\boldsymbol{k}}_i^j\Big)^{\mathrm{T}}\left|v^j\right|\Delta\hat{\boldsymbol{k}}_i^j\,\mathrm{d}\sigma \\ &\quad-\sum_{j=1}^{n}\frac{1}{\alpha_v^j}\int_0^{T_i}\Big(\tilde{\boldsymbol{k}}_{\boldsymbol{v},i}^j\Big)^{\mathrm{T}}\left|v^j\right|\Delta\hat{\boldsymbol{k}}_{\boldsymbol{v},i}^j\,\mathrm{d}\sigma \\ &\quad-\sum_{j=1}^{n}\frac{1}{\alpha_p^j}\int_0^{T_i}\tilde{k}_{p,i}^j\left|v^j\right|\Delta\hat{k}_{p,i}^j\,\mathrm{d}\sigma.\end{aligned} \tag{68}$$

As a result, similar to inequalities (64,65) in case 1 with $t=T_i$, we obtain

$$\Delta V_i\le-\int_0^{T_i}\dot{\boldsymbol{e}}_i^{\mathrm{T}}\,\boldsymbol{K}_{\boldsymbol{e}}\,\dot{\boldsymbol{e}}_i\,\mathrm{d}\sigma\le 0. \tag{69}$$

Combining inequalities (65,69), we see that $\Delta V_i\le 0$ holds in both cases 1 and 2. Consequently, as the initial energy of the human-robot system is bounded, V_i is monotonically decreasing with iterations when $\Delta V_i<0$. Since V_i is defined to be positive, according to the definition of V_i in eq. (41), it indicates that

$$\lim_{i\to\infty}\tilde{\boldsymbol{K}}_{\boldsymbol{s},i}=\lim_{t\to\infty}\tilde{\boldsymbol{K}}_{\boldsymbol{vs},i}=\lim_{t\to\infty}\tilde{\boldsymbol{k}}_{\boldsymbol{ps},i}=\boldsymbol{0}\,. \tag{70}$$

When $\Delta V_i=0$, it gives rise to

$$\dot{\boldsymbol{e}}_i=\ddot{\boldsymbol{e}}_i=\boldsymbol{0} \tag{71}$$

thus

$$\tilde{\boldsymbol{K}}_i\,\boldsymbol{x}_i+\tilde{\boldsymbol{K}}_{\boldsymbol{v},i}\,\dot{\boldsymbol{x}}_i+\tilde{\boldsymbol{k}}_{\boldsymbol{p},i}=\boldsymbol{0} \tag{72}$$

according to eq. (22). As a result, the disturbance can be estimated by the proposed impedance learning method and the robot can follow the desired trajectory of the human in the presence of disturbances. Theorem 2 is thus verified.

ACKNOWLEDGMENT

The authors would like to thank A. Sena and H. Godaba for their careful reading and comments on the manuscript.

REFERENCES

[1] A. Ajoudani, N. Tsagarakis, and A. Bicchi, "Tele-impedance: Teleoperation with impedance regulation using a body–machine interface," *The International Journal of Robotics Research*, vol. 31, no. 13, pp. 1642–1656, 2012.

[2] L. Peternel, N. Tsagarakis, and A. Ajoudani, "A human–robot comanipulation approach based on human sensorimotor information," *IEEE Transactions on Neural Systems and Rehabilitation Engineering*, vol. 25, no. 7, pp. 811–822, 2017.

[3] R. Ikeura and H. Inooka, "Variable impedance control of a robot for cooperation with a human," in *IEEE International Conference on Robotics and Automation*, vol. 3, 1995, pp. 3097–3102.

[4] R. Ikeura, T. Moriguchi, and K. Mizutani, "Optimal variable impedance control for a robot and its application to lifting an object with a human," in *IEEE International Workshop on Robot and Human Interactive Communication*, 2002, pp. 500–505.

[5] Y. Li and S. S. Ge, "Human–robot collaboration based on motion intention estimation," *IEEE/ASME Transactions on Mechatronics*, vol. 19, no. 3, pp. 1007–1014, 2013.

[6] T. Tsumugiwa, R. Yokogawa, and K. Hara, "Variable impedance control based on estimation of human arm stiffness for human-robot cooperative calligraphic task," in *IEEE International Conference on Robotics and Automation*, vol. 1, 2002, pp. 644–650.

[7] C. Mitsantisuk, K. Ohishi, and S. Katsura, "Variable mechanical stiffness control based on human stiffness estimation," in *IEEE International Conference on Mechatronics*, 2011, pp. 731–736.

[8] V. Duchaine and C. M. Gosselin, "General model of human-robot cooperation using a novel velocity based variable impedance control," in *Joint EuroHaptics Conference and Symposium on Haptic Interfaces for Virtual Environment and Teleoperator Systems*, 2007, pp. 446–451.

[9] J. R. Medina and H. Börner and S. Endo and S. Hirche, "Impedance-based Gaussian processes for modeling human motor behavior in physical and non-physical interaction," *IEEE Transactions on Biomedical Engineering*, vol. 66, no. 9, pp. 2499–2511, 2019.

[10] K. Li and H. Zhao and T. Nuchkrua and Y. Yuan and H. Ding, "Sparse bayesian learning-based adaptive impedance control in physical human-robot interaction," in *IEEE International Conference on Robotics and Biomimetics*, 2018, pp. 2379–2385.

[11] X. Xing, K. Maqsood, D. Huang, C. Yang, and Y. Li, "Iterative learning-based robotic controller with prescribed human-robot interaction force," *IEEE Transactions on Automation Science and Engineering*, vol. 33, no. 12, pp. 1705–1709, 2021.

[12] Y. Li, A. Sena, Z. Wang, X. Xing, J. Babic, E. V. Asseldonk, and E. Burdet, "A review on interaction control for contact robots through intent detection," *Progress in Biomedical Engineering*, vol. 4, no. 3, pp. 1–21, 2022.

[13] W. He, S. S. Ge, Y. Li, E. Chew, and Y. S. Ng, "Neural network control of a rehabilitation robot by state and output feedback," *Journal of Intelligent & Robotic Systems*, vol. 80, no. 1, pp. 15–31, 2015.

[14] W. He, C. Xue, X. Yu, Z. Li, and C. Yang, "Admittance-based controller design for physical human-robot interaction in the constrained task space," *IEEE Transactions on Automation Science and Engineering*, vol. 17, no. 4, pp. 1937–1949, 2020.

[15] Y. Li, X. Zhou, J. Zhong, and X. Li, "Robotic impedance learning for robot-assisted physical training," *Frontiers in Robotics and AI*, vol. 6, pp. 1–13, 2019.

[16] Y. Li, G. Ganesh, N. Jarrassé, S. Haddadin, A. Albu-Schaeffer, and E. Burdet, "Force, impedance, and trajectory learning for contact tooling and haptic identification," *IEEE Transactions on Robotics*, vol. 34, no. 5, pp. 1170–1182, 2018.

[17] A. Fayazi, N. Pariz, A. Karimpour, and S. H. Hosseinnia, "Robust position-based impedance control of lightweight single-link flexible robots interacting with the unknown environment via a fractional-order sliding mode controller," *Robotica*, vol. 36, pp. 1920–1942, 2018.

[18] F. Stulp, J. Büchli, A. Ellmer, M. Mistry, E. A. Theodorou, and S. Schaal, "Model-free reinforcement learning of impedance control in stochastic environments," *IEEE Transactions on Autonomous Mental Development*, vol. 4, no. 4, pp. 330–341, 2012.

[19] J. Luo, E. Solowjow, C. Wen, J. A. Ojea, A. M. Agogino, A. Tamar, and P. Abbeel, "Reinforcement learning on variable impedance controller for high-precision robotic assembly," in *International Conference on Robotics and Automation*, 2019, pp. 3080–3087.

[20] R. Martan-Martan, M. A. Lee, R. Gardner, S. Savarese, J. Bohg, and A. Garg, "Variable impedance control in end-effector space: An action space for reinforcement learning in contact-rich tasks," in *IEEE/RSJ International Conference on Intelligent Robots and Systems*, 2019, pp. 1010–1017.

[21] M. Bogdanovic, M. Khadiv, and L. Righetti, "Learning variable impedance control for contact sensitive tasks," *IEEE Robotics and Automation Letters*, vol. 5, no. 4, pp. 6129–6136, 2020.

[22] H. Huang and C. Yang and C. L. P. Chen, "Optimal robot–environment interaction under broad fuzzy neural adaptive control," *IEEE Transactions on Cybernetics*, vol. 51, no. 7, pp. 3824–3835, 2020.

[23] E. Burdet, D. W. Franklin, and T. E. Milner, *Human robotics: neuromechanics and motor control*. MIT Press, 2013.

[24] M. Bin Suleiman, Z. B. Binti Ibrahim, and A. F. N. Bin Rasedee, "Solution of higher-order odes using backward difference method," *Mathematical Problems in Engineering*, vol. 2011, pp. 1–18, 2011.

[25] J.-J. E. Slotine and W. Li, *Applied nonlinear control*. Prentice Hall Englewood Cliffs, NJ, 1991.

[26] C.-L. Chen and Y.-H. Yang, "Position-dependent disturbance rejection using spatial-based adaptive feedback linearization repetitive control," *International Journal of Robust and Nonlinear Control*, vol. 19, no. 12, pp. 1337–1363, 2009.

[27] E. Burdet and R. Osu and D.W. Franklin and T. Yoshioka and T.E. Milner and M. Kawato, "A method for measuring endpoint stiffness during multi-joint arm movements," *Journal of Biomechanics*, vol. 33, no. 12, pp. 1705–1709, 2000.

[28] D. Shen and J. Xu, "Adaptive learning control for nonlinear systems with randomly varying iteration lengths," *IEEE Transactions on Neural Networks and Learning Systems*, vol. 30, no. 4, pp. 1119–1132, 2018.

[29] M. S. D. Queiroz, D. M. Dawson, S. P. Nagarkatti, and F. Zhang, *Lyapunov-based control of mechanical systems*. Springer, 2012.

Xueyan Xing received the B.S. degree in automation from Northeastern University, Shenyang, China, in 2015, the M.S. degree in control engineering from the Harbin Institute of Technology, Harbin, China, in 2017, and the Ph.D. degree in control theory and control engineering from Beihang University, Beijing, China, in 2020. She was a research fellow with the Department of Engineering and Design, University of Sussex, Brighton, U.K from 2020 to 2022. Currently, she is a research fellow with the Continental-NTU Corporate Lab, Nanyang Technological University, Singapore. Her current research interests include physical human-robot interaction, distributed control and optimization, and vibration control.

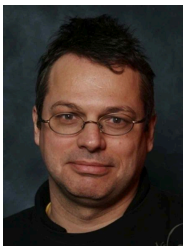

Etienne Burdet received the M.S. degree in mathematics in 1990, the M.S. degree in physics in 1991, and the Ph.D. degree in robotics from ETH-Zurich, Switzerland in 1996. He is currently a Professor and Chair of Human Robotics with Imperial College London. His main research interest is in human-machine interaction. He uses an integrative approach of neuroscience and robotics to investigate human sensorimotor control, and to design efficient assistive devices and training systems for neuro-rehabilitation, which are tested in clinical trials and commercialized.

Weiyong Si received the M.S. degree in aerospace engineering from the Beijing Institute of Technology, China, in 2018. He is currently pursuing PhD degree in robotics at Bristol Robotics Laboratory and the University of the West of England, Bristol. His research interests include robot skill learning, teleoperation and robot control.

Chenguang Yang (M'10-SM'16) received the Ph.D. degree in control engineering from the National University of Singapore, Singapore, in 2010, and postdoctoral training in human robotics from the Imperial College London, London, U.K. He was awarded UK EPSRC UKRI Innovation Fellowship and individual EU Marie Curie International Incoming Fellowship. As the lead author, he won the IEEE Transactions on Robotics Best Paper Award (2012) and IEEE Transactions on Neural Networks and Learning Systems Outstanding Paper Award (2022). He is the Corresponding Co-Chair of IEEE Technical Committee on Collaborative Automation for Flexible Manufacturing, a Fellow of Institute of Engineering and Technology (IET), a Fellow of Institution of Mechanical Engineers (IMechE), and a Fellow of British Computer Society (BCS). His research interest lies in human robot interaction and intelligent system design.

Yanan Li (M'14-SM'21) received the B.Eng. and M.Eng. degrees in automatic control from the Harbin Institute of Technology, China, in 2006 and 2008, respectively, and the Ph.D. degree in robotics from the National University of Singapore, Singapore, in 2013. From 2015 to 2017, he was a Research Associate with the Department of Bioengineering, Imperial College London, London, U.K. From 2013 to 2015, he was a Research Scientist with the Institute for Infocomm Research, Agency for Science, Technology and Research, Singapore. He is currently a Senior Lecturer in control engineering with the Department of Engineering and Design, University of Sussex, Brighton, U.K. His general research interests include human-robot interaction, robot control, and control theory and applications.